Properties of the Liquid-Vapor Interface of Acetone-Water Mixtures. A Computer Simulation and ITIM Analysis Study

Balázs Fábián,[1,2] Balázs Jójárt,[3] George Horvai,[2,4] and Pál Jedlovszky[1,4,5,*]

[1]*Laboratory of Interfaces and Nanosize Systems, Institute of Chemistry, Eötvös Loránd University, Pázmány P. Stny 1/A, H-1117 Budapest, Hungary*

[2]*Department of Inorganic and Analytical Chemistry, Budapest University of Technology and Economics, Szt. Gellért tér 4, H-1111 Budapest, Hungary*

[3]*Department of Chemical Informatics, Faculty of Education, University of Szeged, Boldogasszony sgt. 6. H-6725 Szeged, Hungary*

[4]*MTA-BME Research Group of Technical Analytical Chemistry, Szt. Gellért tér 4, H-1111 Budapest, Hungary*

[5]*EKF Department of Chemistry, Leányka utca 6, H-3300 Eger, Hungary*

Running title: Liquid-Vapor Interface of Acetone-Water Mixtures

*Electronic mail: pali@chem.elte.hu

Abstract

Molecular dynamics simulations of the liquid-vapor interface of acetone-water mixtures of different compositions, covering the entire composition range have been performed on the canonical (N,V,T) ensemble at 298 K, using a model combination that excellently describes the mixing properties of these compounds. The properties of the intrinsic liquid surfaces have been analyzed in terms of the Identification of the Truly Interfacial Molecules (ITIM) method. Thus, the composition, width, roughness and separation of the subsurface molecular layers as well as self-association, orientation, and dynamics of exchange with the bulk phase of the surface molecules have been analyzed in detail. Our results show that acetone molecules are strongly adsorbed at the liquid surface, and this adsorption extends to several molecular layers. Like molecules in the surface layer are found to form relatively large lateral self-associates. The effect of the vicinity of the vapor phase on a number of properties of the liquid phase vanishes beyond the first molecular layer, the second subsurface layer being already part of the bulk liquid phase in these respects. The orientational preferences of the surface molecules are governed primarily by the dipole-dipole interaction of the neighboring acetone molecules, and hydrogen bonding interaction of the neighboring acetone-water pairs.

1. Introduction

Acetone is a prototypical example of strongly polar but aprotic organic solvents. Although the acetone molecule lacks H atoms to be donated, it can act as a H-acceptor partner in hydrogen bonds. Therefore, upon adding to acetone H-donor co-solvents, such as water or methanol, the physico-chemical properties of these mixtures can be fine tuned by the amount of hydrogen bonds formed in the system via controlling the molar ratio of the different components. As a consequence, neat acetone as well as acetone-water and acetone-methanol mixtures are important reaction media both in preparative organic chemistry and in the chemical industry.

The solvation properties of such mixtures are strongly related to the ratio of the apolar CH_3, strongly polar but aprotic C=O, and H-donor OH groups in the system. The interplay of these groups of markedly different chemical character is, however, severely altered at the vicinity of an interface with an apolar phase, such as at the free surface of the liquid. As a consequence, the molecular level structure, and hence also the solvation properties of such systems might be markedly different at the liquid-vapor and at liquid-liquid interfaces than in the bulk liquid phase. This fact can be of great importance in the field of heterogeneous reactions and, in particular, heterogeneous catalysis. In spite of this importance, however, little is known about the molecular level properties of the liquid-vapor interface of acetone-water mixtures.

In studying molecular level properties of disordered systems, experimental studies can be well complemented by computer simulation investigations, since in a simulation a detailed, three-dimensional insight at the molecular level is obtained into an appropriately chosen model of the system of interest.[1] Although numerous computer simulation studies of the bulk liquid phase of neat acetone[2-6] as well as of its mixtures with water[7-18] and other co-solvents,[9,19-25] being sometimes in supercritical state[12,22] have been reported in the past decades, little is known about the behavior of acetone at interfaces. In fact, although the properties of the acetone molecules adsorbed at the surface of ice,[26,27] mixed acetone-water nanoclusters,[28] the liquid-vapor interface of neat acetone[29-31] and acetone-methanol mixtures of various compositions[32] have already been investigated by computer simulation methods several times, and the liquid-vapor interface of neat acetone[29,33] as well as of acetone-water mixtures[34,35] have also been studied, although scarcely, by surface sensitive experimental

methods, we are not aware of any detailed computer simulation investigation of the liquid-vapor interface of acetone-water mixtures.

The lack of such simulation studies clearly originates from the difficulties arising in reproducing the experimentally well known full miscibility of acetone and water in computer simulations. In fact, the mixing of acetone and water is only accompanied by a very small (~0.5 kJ/mol) decrease of the free energy,[36] and hence, the thermodynamic driving force being behind their full miscibility is very weak. As it was shown by Perera and Sokolić, the OPLS model of acetone[37] demixes from several widely used water models in bulk phase computer simulations, given that the simulation is running for a long enough time.[13] In subsequent studies it was also shown that more recent acetone models, such as the KBFF,[11] TraPPE,[38] and AUA4[39] models are not fully miscible either with a number of conventionally used water models.[15,17] The free energy difference between the mixed and demixed states is always very small, being below 1-2 kJ/mol, and hence being closer to the experimental value than *RT*, however, the simulated free energy difference always turned out to be positive in contrast with the negative experimental value.[17]

It should also be noted that in bulk phase simulations demixing is suppressed and delayed by the use of periodic boundary conditions. Therefore, in short enough simulations the non-miscibility of the components might not even be noticed. In contrast, in the presence of an apolar object, such as a liquid-vapor interface, demixing occurs very quickly, and thus the non-miscibility of the two components becomes immediately evident.

Recently we found an acetone-water model combination, namely the Pereyra-Asar-Carignano (PAC) model of acetone[16] and the TIP5P-E model of water[40] that are not only fully miscible with each other, but also reproduce the experimental free energy, energy and entropy of mixing values very accurately in the entire composition range.[17] The PAC model is based on the idea that reproduction of the full miscibility requires the modeling of the polarization of the acetone molecule due to the nearby waters.[16] Therefore, the fractional charges used in the PAC model are scaled according to the molar ratio of acetone and water in the mixture, which limits the use of this acetone model solely to acetone-water binary systems. Nevertheless, this model pair should be suitable for the simulation of the liquid-vapor interface of acetone-water mixtures.

In simulating fluid (i.e., liquid-liquid and liquid-vapor) interfaces one has to face the difficulty that when such interfaces are seen in molecular resolution (such as in atomistic simulations), the exact location of the interface is not easy to determine. The problem originates from the fact that such interfaces are corrugated, on molecular length scales, by

capillary waves. Approximating the interfacial region by a slab parallel with the Gibbs dividing surface was repeatedly shown to lead to a systematic error of unknown magnitude in the structural properties as well as composition of the interfacial layer,[41-46] and even propagates to the thermodynamic properties of the binary system.[47] Following the pioneering paper of Chacón and Tarazona,[48] several methods have been proposed to circumvent this problem and to detect the real, capillary wave corrugated, intrinsic liquid surface.[41,49-54] Among them, the method of Identification of the Truly Interfacial Molecules (ITIM)[41] turned out to be an excellent compromise between computational cost and accuracy.[53]

In an ITIM analysis probe spheres of a given radius are moved along test lines perpendicular to the macroscopic plane of the interface from the bulk opposite phase towards the surface of the phase of interest. Once the probe sphere touches the first molecule of the phase of interest, this molecule is marked as interfacial, and the probe starts to be moved along the next test line. Once all test lines are considered, the full list of the truly interfacial molecules (i.e., the ones "seen" by the probe from the opposite phase) is determined. Further, by disregarding the full set of molecules identified as constituting the surface layer and repeating the entire procedure the molecules constituting the subsequent (second, third, etc.) molecular layers beneath the liquid surface can also be determined.[41] The ITIM method has successfully been applied to the liquid-vapor interface of various neat[31,41,55] and binary molecular systems,[32,43-46,56] room temperature ionic liquids,[57-60] and to various liquid-liquid interfaces.[42,47,61,62] Furthermore, using the ITIM method one of the so far unexplained anomalies of water, namely the surface tension anomaly has recently been successfully explained.[63,64]

In this paper we present a detailed analysis of the liquid-vapor interface of acetone-water mixtures of different compositions, covering the entire composition range from neat water to neat acetone, using molecular dynamics computer simulation and ITIM surface analysis. In order to maintain the full miscibility of the two components, the simulations are performed using the PAC model of acetone and TIP5P-E model of water. The results are analyzed both in terms of the properties of the intrinsic surface itself (e.g., width, roughness, composition, lateral inhomogeneities, separation of the subsequent layers) and of the properties of the surface molecules (orientation, dynamics of exchange with the bulk phase). The results are compared with those obtained previously for other aqueous binary mixtures[43-46] as well as for mixtures of acetone with methanol.[32]

The paper is organized as follows. In sec. 2., details of the calculations performed, including both the molecular dynamics simulations and the ITIM analyses are given. The

obtained results concerning the properties of the entire subsurface molecular layers and of the surface molecules are discussed in detail in secs. 3 and 4, respectively. Finally, in sec. 5, the main conclusions of this study are summarized.

2. Computational Details

2.1. Molecular Dynamics Simulations. Molecular dynamics simulations of the liquid-vapor interface of acetone-water mixtures of 11 different compositions, including the two neat systems, have been performed on the canonical (*N*,*V*,*T*) ensemble at the temperature of 298 K. The *X*, *Y* and *Z* edges of the rectangular basic simulation box have been 400, 50 and 50 Å long, respectively, *X* being the macroscopic surface normal. The basic box has consisted of 4000 molecules, among which 9, 400, 800, 1200, 1600, 2000, 2400, 2800, 3200, 3600, and 4000 respectively, have been acetone in the different systems. These systems are referred to here as the 0%, 10%, 20%, 30%, 40%, 50%, 60%, 70%, 80%, 90%, and 100% acetone system, respectively.

Acetone and water molecules have been modeled by the PAC[16] and TIP5P-E[40] potentials, respectively. Thus, the internal energy of the entire system has been calculated as the sum of all pair interaction energies, and the pair interaction energy of the *i*th and *j*th molecule, u_{ij}, has been calculated as the sum of the Lennard-Jones and charge-charge Coulomb contributions of all the pairs of their interaction sites:

$$u_{ij} = \sum_{A}^{n_i} \sum_{B}^{n_j} \frac{1}{4\pi \in_0} \frac{q_A q_B}{r_{iA,\,jB}} + 4\varepsilon_{AB}\left[\left(\frac{\sigma_{AB}}{r_{iA,\,jB}}\right)^{12} - \left(\frac{\sigma_{AB}}{r_{iA,\,jB}}\right)^{6}\right]. \qquad (1)$$

In this equation, indices *A* and *B* run over the N_i and N_j interaction sites of molecules *i* and *j*, respectively, q_A and q_B are the fractional charges located at the respective sites, $\in_0$ is the vacuum permittivity, $r_{iA,jB}$ is the distance between site *A* of molecule *i* and site *B* of molecule *j*, and σ_{AB} and ε_{AB} are the Lennard-Jones distance and energy parameters, respectively, of the site pair *A* and *B*, related to the values characteristic to the individual sites through the Lorentz-Berthelot rule,[1] namely

$$\sigma_{ab} = \frac{\sigma_a + \sigma_b}{2} \qquad (3)$$

and

$$\varepsilon_{ab} = \sqrt{\varepsilon_a \varepsilon_b} \ . \tag{2}$$

The interaction of the molecule pair *i* and *j* has been truncated to zero beyond the center-center cut-off distance of 15 Å. The long range part of the electrostatic interaction has been accounted for by means of the Particle Mesh Ewald method.[65]

The σ, ε and q interaction parameters, listed in Table 1 for both molecular models used, are composition independent, apart from the fractional charges of the acetone molecule, which depend on the mole fraction of acetone in the system, x_{ac}, as

$$q(x_{ac}) = q(1)\,(1.1502 - 0.2385\,x_{ac} + 0.0883\,x_{ac}^2)\,, \tag{4}$$

where $q(1)$ stands for the fractional charge values corresponding to the acetone mole fraction of 1, i.e., neat acetone.[16]

The PAC acetone model consists of ten interaction sites, corresponding to the ten atoms of the acetone molecule.[16] The TIP5P-E model is, on the other hand, built up by five interaction sites, three of which corresponds to the O and H atoms of the water molecule, whereas the other two, denoted conventionally as L, are non-atomic interaction sites, located in the directions of the two lone pairs of the O atom. Hence, the two L sites and two H atoms are arranged in tetrahedral directions around the central O atom of the water molecule.[40] Both types of molecules have been kept rigid in the simulations by means of the LINCS[66] algorithm. The bond lengths and bond angles of the two molecular models are collected in Table 2.

The simulations have been performed using the GROMACS 4.5.5 program package.[67] Equations of motion have been integrated in time steps of 2 fs. The temperature of the systems has been controlled by means of the weak coupling algorithm of Berendsen et al.[68] To prepare the starting configurations the required number of molecules have been placed in a rectangular basic box, the length of the *X* edge of which has roughly corresponded to the liquid density of the given mixture (edges *Y* and *Z* have already been set to 50 Å).The systems have been energy minimized and equilibrated for 4 ns at constant pressure (1 bar), allowing only the *X* edge of the basic box to change. The interfacial systems have then been created by increasing the *X* edge of the basic box to its final value of 400 Å. The interfacial systems have been further equilibrated, on the canonical ensemble, for 5 ns. Then, in the course of the 2 ns long production runs, 2000 sample configurations, separated from each other by 1 ps long trajectories, have been dumped for further analyses.

2.2. ITIM Analyses. In the ITIM analyses the first three consecutive molecular layers beneath the liquid surface have been determined for each system. The radius of the spherical probe has been 2 Å, in order to keep the probe in the size range comparable with that of the atoms.[41] The probe has been moved along a set of test lines arranged in a 100×100 grid in the macroscopic plane of the interface, *YZ*. Thus, the distance of two neighboring test lines has been 0.5 Å, in accordance with the suggestion of Jorge et al.[53] To determine the point where the probe sphere touches an atom, the diameters of the atoms have been estimated by their Lennard-Jones distance parameter, σ (see Table 1). Once the entire surface layer was identified, it was discarded and the whole procedure has been repeated twice more, hence, the molecules constituting the second and third layers beneath the liquid surface have also been identified. An equilibrium snapshot of the 10% acetone system is shown in Figure 1, indicating also the first three molecular layers beneath the liquid surface. All the calculated properties have been averaged not only over the 2000 sample configurations per system, but also over the two liquid surfaces present in the basic box.

3. Properties of the Subsurface Molecular Layers

3.1. Composition and Its Inhomogeneities. To investigate the possible adsorption of acetone at the surface of acetone-water mixtures we have plotted the composition of the first three molecular layers beneath the liquid surface (in terms of acetone mole percentage) as a function of the bulk phase composition in Figure 2. For this purpose, the entire system beneath the third molecular layer has been regarded as the bulk liquid phase. As is seen, the acetone content of the surface layer is considerably higher than that of the bulk liquid phase, and this effect is more pronounced at low bulk phase acetone mole fractions. Thus, in the 10% acetone system the bulk liquid phase consists of 6.2 mole% acetone, which is almost an order of magnitude smaller than the 50 mole% acetone content of the surface layer of the same system. It is also rather interesting that the composition of the surface layer behaves in a rather similar way as the composition of the vapor phase being in equilibrium with the liquid mixture. To demonstrate this, we also added the experimental vapor phase composition[69] as a function of the liquid phase composition to Fig. 2. As is seen, in spite of the difference between the real system and the model used here, and of the fact that the surface layer of the liquid phase does not necesserily have the same composition as the vapor phase, the shape of the two curves are remarkably similar. It is also seen that up to about 70 mole% bulk phase acetone content the second and even the third layer beneath the surface is noticeably richer in

acetone than the bulk liquid phase. The acetone mole percentage values in the first three layers beneath the surface as well as in the bulk liquid phase of the systems simulated are summarized in Table 3.

The observed strong adsorption ability, extending to several subsurface molecular layers, is typical of strongly dipolar solutes in aqueous systems. Thus, similar behavior was previously observed in the aqueous solutions of acetonitrile[44] and HCN,[46] in a clear contrast with the adsorption of methanol[43] or dimethyl sulfoxide (DMSO)[45] at the surface of their aqueous solutions, which is strictly restricted to one molecular layer. Further, the behavior of acetone in these aqueous systems is in a marked contrast with that in mixtures with methanol, in which practically no adsorption was observed.[32] The strong adsorption ability of acetone in aqueous solutions is clearly related to the presence of the apolar CH_3 groups of the acetone molecule, whereas the multilayer character of the adsorption indicates that dipolar forces are likely to play an important role at the liquid surface. This point is further addressed in a following sub-section of this paper.

The observed adsorption behavior of the acetone molecules inevitably raises the question of the reliability of the acetone model used in the simulations. As it has been described in detail in sec. 2.1, the used PAC model of acetone bears fractional charges depending on the acetone/water mole fraction of the system. The adsorption of acetone at the surface, however, means that the composition of the surface layer does not correspond to the acetone fractional charges used. Therefore, before performing any further analyses, the relevance of the simulated configurations to be analyzed has to be verified. To do this, we have calculated the surface tension, γ, of the simulated systems, and compared them to the experimental values.[70] The calculated and experimental surface tension data are collected in Table 3. As is seen, the simulation $\gamma(x_{ac})$ data follows the curvature of the experimental results, with a shift to about 4-6 mN/m smaller values. This shift simply reflects the fact that the two potential models used underestimate the surface tension of the neat liquids. To demonstrate that, apart from this shift, the simulated $\gamma(x_{ac})$ data follows well the experimental curve we show the comparison of the two data sets normalized by the surface tension of neat acetone, γ_{ac}, in Figure 3. To further demonstrate that the results obtained from our simulations are relevant to the surface of acetone-water mixtures, we have repeated the simulations of the 10% and 50% acetone systems, using the acetone fractional charges corresponding to the composition of the surface layer rather than to the entire system. The use of this surface-fixed charge set, however, did not change any of our qualitative conclusions.

The strong adsorption ability of the acetone molecules indicate that, in spite of the full miscibility of acetone and water, the unlike molecules tend to separate from each other on a microscopic length scale along the surface normal axis. This separation is induced by the different energy cost of the two molecules being in contact with an apolar phase. It is also interesting to see, however, if the acetone and water are also separated microscopically from each other at the liquid surface in the lack of such an external driving force, in other words, whether they form relatively large self-associates within the surface layer. Formation of self-associates of like molecules in binary systems can be investigated by means of Voronoi analysis.[71] In a two-dimensional system of seeds (e.g., molecules at a surface) the Voronoi polygon (VP) of a seed is the locus of the points that are closer to this particular seed than to any other one.[72,73] Given that the seeds are homogeneously distributed, the area distribution of their VP follows a Gaussian shape, whereas in the presence of inhomogeneities (i.e., clusters of nearby seeds and large empty areas) the VP area distribution exhibits a peak with a long, exponentially decaying tail at its large area side.[74] Therefore, in binary systems where the like components form self-associates, the VP are distribution obtained by disregarding the molecules of one of the two components, and taking only those of the other one into account, also exhibits the exponentially decaying tail at large area values (as the areas occupied by the self-associates of the disregarded component are converted to empty areas this way).[75] To characterize the extent of self-association of the like molecules at the surface of acetone-water mixtures we have projected the center (i.e., carboxylic C and O atom for acetone and water, respectively) of each surface molecule to the macroscopic plane of the liquid surface, *YZ*, and performed VP analysis on these projections. The distributions of the VP area, *A*, have been determined in three different ways, i.e., taking both types of molecules into account, taking only acetone molecules into account while disregarding the water molecules, and taking only water molecules into account while disregarding the acetone molecules. The VP area distributions, $P(A)$, obtained in these three ways in selected systems are shown in Figure 4. To emphasize the exponential decay of the large area tail in some cases, the $P(A)$ distributions are shown on a logarithmic scale, while the inset shows the three distributions obtained in the 10% acetone system on a linear scale.

As is seen, when both types of molecules are taken into account, the VP area distribution is always a narrow Gaussian, reflecting simply the trivial fact that the liquid surface is uniformly covered by the surface molecules. However, when water molecules are disregarded and only acetones are taken into account, the $P(A)$ distributions increasingly deviate from the Gaussian shape with decreasing acetone mole fraction. This effect is even

more pronounced when acetone molecules are disregarded and only waters are taken into account. The finding that the $P(A)$ distributions are, in general, broader, having a longer tail at large A values when the acetone molecules are disregarded then when only acetones are taken into account simply reflects the fact that in the surface layer of the mixed systems simulated water is always the minor component (see Fig. 2 and Table 3). Nevertheless, the self-association ability of the like molecules is clearly revealed. This self-association is illustrated in Figure 5, showing the projections of the centers of the surface molecules to the plane of the macroscopic surface, *YZ*, in equilibrium snapshots of the 10% and 60% acetone systems.

The extent of this self-association can be quantified by calculating the average and largest number of like molecules that form such self-associates. These values can be estimated by dividing the area of the average size and largest circular void, respectively, obtained when one of the two components is disregarded (as these are the areas occupied by an average size and the largest self-associate, respectively, of the disregarded component) by the average VP area in the neat system of this, previously disregarded component. This way, the average size and largest self-associates of water, respectively, are estimated to consist of 5.5 and 8.5 water molecules at the surface of the 10%, 4 and 5.5 water molecules at the surface of the 50%, and 3.5 and 5 water molecules at the surface of the 90% acetone system. Similarly, at the surface of the 10% and 50% acetone systems the average size and largest acetone self-associates consist of 3 and 6, and 8 and 16 acetone molecules, respectively.

3.2. Width, Separation, and Roughness. Figure 6 shows the number density profiles of the acetone and water molecules along the macroscopic surface normal axis, *X*, as well as the mass density profile of the entire system and of its surface layer in systems of selected compositions. Further, Figure 7 shows the mass density profile of the first three layers together with that of the entire system in systems of selected compositions. As is seen, the density peak of the surface layer extends well into the *X* range where the mass density of the system is already constant. Further, the density peak of the second and even the third layer beneath the liquid surface extends into the *X* range of intermediate densities between the values characteristic to the two bulk phases. This finding demonstrates the extent of systematic error caused by a non-intrinsic treatment of the liquid-vapor interface (i.e., its definition as the intermediate density region along the *X* axis), and stresses the importance of using intrinsic analysis in detecting and defining the surface of a liquid phase in computer simulations. It is also seen that although at low acetone contents the acetone density profile exhibits a subsurface peak, corresponding to the aforementioned adsorption of the acetone

molecules at the liquid surface, no such peak is seen, e.g., in the 70% acetone system, where both the acetone and the water density profile change smoothly from the bulk liquid phase value to zero, in spite of the fact that the acetone molecules are adsorbed also at the surface of this system. This fact emphasizes again the importance of using intrinsic surface analysis in simulations of fluid interfaces.

The density profile of the surface molecular layers turns out to be of Gaussian shape in every case, in accordance with the theoretical considerations of Chowdhary and Ladanyi.[76] Thus, fitting a Gaussian function to the simulated density profiles the center and width parameter of the fitted function, X_c and δ, respectively, can serve as an estimate of the average position of the corresponding molecular layer along the macroscopic surface normal axis, and of its average width, respectively. Further, the difference of the X_c values of two consecutive layers, ΔX_c, is an estimate of the average separation of these layers. The X_c, ΔX_c, and δ values corresponding to the first three subsurface layers of all systems simulated are collected in Table 4.

As is seen, the subsurface molecular layers become, in general, broader with increasing acetone content. Thus, the first three layers of the 50% and 90% acetone systems are, on average, 60-70% and 140% broader than those of the 10% acetone system. Similarly, the average separation of two subsequent molecular layers also increases steadily with increasing acetone mole fraction. These findings can, in general, simply be explained by the larger size of the acetone molecule as compared to water. Interestingly, however, the widths of the first three subsurface layers of neat acetone are considerably, about 30% smaller than those of the 90% acetone system, instead, they roughly equal with those of the 60% acetone system. This finding suggests that although both water and acetone molecules can form tightly packed structures in the absence of the other component, water and acetone molecules cannot be as tightly packed together as either of them with like molecules. This view is supported by the fact that the mixing of the acetone and water molecules is energetically unfavorable at high acetone mole fractions,[36] and also by our previous observation that relatively large lateral self-associates of the like molecules are formed in the surface layer of the mixed systems.

It is also seen that both the second and the third layer beneath the surface are somewhat (i.e., typically by about 3-5%) narrower than the surface molecular layer, whereas no such clear trend is seen between the widths of the second and third layers. Further, the average separation of the first two molecular layers is always larger than that of the second and third layers, and this difference decreases with increasing acetone concentration from

about 13% (neat water) to 1.5% (neat acetone). These findings reflect the fact that, similarly to other systems,[31,32,42,46] the vicinity of a low density phase loosens the packing of the surface molecules, but this effect does not extend beyond the first molecular layer beneath the surface. Further, this effect is stronger for water, in which the hydrogen bonding network of the molecules results in an unusually tight packing of the bulk liquid phase, than in acetone, in which no such network exists.

It is also interesting to compare the density profiles of the acetone and water molecules within the surface layer. Such a comparison is shown for systems of selected compositions in Figure 8. For the sake of better comparison, the height of the acetone and water number density peaks are always scaled to each other; the position of the acetone and water molecules are represented by that of their central C and O atom, respectively.

As is seen, in the 10% acetone system, in which the surface layer consists of 60% acetone, the water and acetone density peaks exactly coincide. On the other hand, in systems of higher acetone content, in which water is the minor component of the surface layer, surface water molecules are located, on average, somewhat closer to the vapor phase than surface acetones. Similar behavior of the surface minor component was previously observed in water-methanol[43] and water-DMSO[45] mixtures. By contrast, in mixtures of water with HCN,[46] and acetone with methanol,[32] always the same component (i.e., HCN and methanol, respectively) was found to be located somewhat closer to the vapor phase within the surface layer, independently from its composition.

Having the full list of the interfacial molecules determined, the molecular scale roughness of the liquid surface can also be described. Clearly, the characterization of a wavy surface requires the use of at least two parameters, i.e., a frequency-like and an amplitude-like one. For this purpose, we proposed to use the parameter pair ξ and a, which can be determined in the following way.[56] The average normal distance of two surface points, $\bar{d}$, (i.e., their distance along the macroscopic surface normal axis, X) exhibits a saturation curve as a function of the lateral distance of these points, l (i.e., their distance within the macroscopic plane of the surface, YZ). The $\bar{d}(l)$ data can be reasonably well fitted by the following function, formally analogous with the Langmuir isotherm:

$$\bar{d} = \frac{a\xi l}{a + \xi l}. \tag{4}$$

Thus, ξ is the steepness of the $\bar{d}(l)$ curve at small lateral distances, where this curve is practically linear, and hence it is a frequency-related parameter, whereas a is the saturation value of $\bar{d}$ at large lateral distances, and hence it is an amplitude-related parameter.[56]

The ξ and a roughness parameters corresponding to the first three molecular layers beneath the liquid surface of the systems simulated are collected in Table 4, whereas the $\bar{d}(l)$ roughness curves of the first layer of selected systems are shown in Figure 9. Although the obtained ξ and a values are rather noisy as a function of the composition of the system, it is clear again that, in general, the surface layer becomes rougher, both in terms of ξ and a, with increasing acetone concentration, but in neat acetone the roughness of the liquid surface is smaller than in the acetone-water mixtures. These findings are again likely to be related to the larger size of the acetone than the water molecule, and the relatively loose packing of the unlike molecules at the liquid surface.

A marked difference is seen, however, between the roughness of the first and subsequent molecular layers, the first layer being rougher, both in terms of ξ and a, than the second and the third one, while the roughness of these latter two layers are already rather similar to each other in every system. This is illustrated in the inset of Fig. 9, showing the $\bar{d}(l)$ roughness curves of the first three subsurface molecular layers of the 70% acetone system. This finding emphasizes again that the loosening effect of the vicinity of the low density vapor phase on the packing of the surface molecules vanishes beyond the first molecular layer at the liquid surface.

4. Properties of the Surface Molecules

4.1. Dynamics of Exchange between the Surface and the Bulk. The dynamics of exchange of the molecules between the surface layer and the bulk liquid phase can be characterized by the survival probability of the molecules within the surface layer. The survival probability, $L(t)$, is simply the probability that a molecule that belongs to the surface layer at t_0 remains at the surface up to $t_0 + t$. Since molecules might seemingly leave the surface layer at certain instances due to some oscillatory moves, this situation has to be distinguished from the case when a molecule indeed leaves the surface layer and enters permanently to the bulk liquid phase. Therefore, departure of a molecule from the surface layer between t_0 and $t_0 + t$ is allowed given that it returns to the surface within the time of Δt. Here we set this Δt time window to 2 ps, in accordance with the characteristic time of the

oscillatory moves of the molecules. However, to avoid the arbitrariness of the results introduced by this particular choice of Δt, we have repeated all the analyses using the Δt value of 1 ps, as well. It should be noted that since the saved sample configurations are separated from each other by 1 ps long trajectories, the choice of $\Delta t = 1$ ps means that, in fact, no departure of a molecule from the surface is allowed, while in the case of $\Delta t = 2$ ps a molecule cannot be absent from the surface layer in two consecutive sample configurations between t_0 and $t_0 + t$. However, the particular choice of Δt did not change any of our conclusions, therefore, here we only present results corresponding to the choice of $\Delta t = 2$ ps.

The $L(t)$ survival probability curves are shown in Figure 10 as obtained both for the acetone and water molecules in the surface layer of systems of selected compositions. Since the departure of a molecule from the liquid surface is a process of first order kinetics, the obtained $L(t)$ data are of exponential decay. To emphasize the exponential character of this decay, the inset of Fig. 10 shows the $L(t)$ curves of the water and acetone molecules of the first three subsurface layers of the 50% acetone system on a logarithmic scale. Fitting the function $\exp(-t/\tau)$ to the simulated $L(t)$ data provides the mean residence time of the molecules in the surface layer, τ. The τ values obtained for both types of molecules in the first three subsurface layers of the systems simulated are collected in Table 4.

As is seen, acetone molecules stay at the liquid surface considerably longer than waters. Further, the mean residence time of the acetone molecules decreases with increasing acetone mole fraction, whereas for water it is independent from the composition of the system, being typically about 9-10 ps. Thus, the mean surface residence time of the acetone molecules at the surface of the 10% acetone system is about eight times larger than that of the water molecules, while this ratio decreases to 2-3 in the systems of higher acetone content. The insensitivity of the surface residence time of the water molecules to the surface composition is likely related to the previously observed self-association of the surface water molecules. Thus, a surface water molecule is typically located within such a self-associate, being surrounded by several water neighbors to which it can hydrogen bond, independently from the overall composition of the surface layer.

It is also seen that the mean residence time values in the second and third molecular layers beneath the surface are about an order of magnitude smaller than in the surface layer in every case. Furthermore, these values are comparable with the length of the Δt time window of 2 ps, allowed for the molecules to be absent from the layer. This finding indicates that, from the dynamical point of view, the effect of the vicinity of the vapor phase does not extend

beyond the first molecular layer beneath the liquid surface; in this respect, the second subsurface molecular layer is already part of the bulk liquid phase.

4.2. Orientation at the Surface. To fully characterize the orientation of rigid molecules relative to an external direction (or surface) one needs to calculate the bivariate joint probability distribution of two independent orientational variables.[77,78] We have shown that the angular polar coordinates ϑ and ϕ of the external direction (surface normal vector) in a local Cartesian frame fixed to the individual molecules represents a sufficient choice of such a parameter pair.[77,78] Further, since ϑ is an angle between two general spatial vectors (i.e., the *z* axis of the local frame and the surface normal), whereas ϕ is an angle of two vectors restricted, by definition, to lay in a given plane (i.e., the *xy* plane of the local frame), uncorrelated orientation of the molecules with the surface only results in a uniform distribution if $\cos\vartheta$ and ϕ are chosen to be the independent variables.

Here we define the local frames fixed to the acetone and water molecules in the following way. Their axis z coincides with the main symmetry axis of the corresponding molecule, pointing along the molecular dipole vector (i.e., the *z* coordinates of the acetone CH_3 and water H atoms are positive), *x* is the molecular normal, and *y* is perpendicular to the above two axes. The surface normal vector, $\underline{X}$, is pointing, to our convention, from the liquid to the vapor phase. Due to the C_{2v} symmetry of both the acetone and the water molecule, the local frame is always chosen in such a way that the relation $0^o \le \phi \le 90^o$ holds. The definition of these local Cartesian frames as well as of the polar angles ϑ and ϕ is illustrated in Figure 11.

In order to take the effect of the local curvature of the surface on the orientational preferences of the surface molecules also into account, we have divided the surface layer according to its mass density profile into three separate zones, marked by A, B, and C, respectively. Thus, zones A and C cover the *X* ranges at the vapor and liquid sides of the density peak, respectively, in which the surface layer mass density is below the half of its maximum value, whereas zone B corresponds to the *X* range where the surface layer mass density exceeds the half of its maximum value. Thus, zones A and C typically correspond to the crests and troughs of the molecularly rugged surface, in other words, to surface portions of locally convex and concave curvatures, respectively. The division of the surface layer to zones A, B, and C is also illustrated in Fig. 11.

The $P(\cos\vartheta,\phi)$ orientational maps of the water and acetone molecules are shown in Figures 12 and 13, respectively, as obtained at the surface of the corresponding neat system as well as of mixed systems of selected compositions. In addition to results corresponding to the entire surface layer, those obtained in its separate zones A, B, and C are also shown. As is seen, at the surface of both neat liquids the molecules prefer nearly parallel dipolar alignments with the surface plane, as reflected from the relatively high probabilities of the $\cos\vartheta \sim 0$ orientations. In water, the preferred orientation, marked by I_w, corresponds to the $\{\cos\vartheta = 0;\ \phi = 0^o\}$ point of the orientational map. In this orientation, the water molecule stays parallel with the macroscopic plane of the liquid surface, *YZ*. As is seen, this orientation is preferred in the entire surface layer as well as in its zone B. On the other hand, in zones A and C the water molecules have markedly different orientational preferences. Thus, in zone A, i.e., at the tips of the crests of the wavy surface the main peak of the distribution I_w is shifted to somewhat lower $\cos\vartheta$ values, and thus it is located around $\cos\vartheta = -0.3$ and $\phi = 0^o$. This orientation corresponds to a tilted alignment of the water molecule, in which the dipole vector points flatly towards the liquid phase. To emphasize this tilt in zone A, this orientation is referred to here as I_w^A. Further, in zone A another orientation, corresponding to the $\{\cos\vartheta = 0.3;\ \phi = 90^o\}$ point of the map is also preferred by the water molecules. In this orientation, marked as II_w, the water molecule stays perpendicular to the liquid surface pointing by one of its H atoms straight to the vapor phase. In zone C (i.e., bottom of the troughs of the wavy surface) the water molecules also have a dual orientational preference. Thus, the main peak of the map of the entire surface layer shifts here to somewhat lower $\cos\vartheta$ values, appearing around $\{\cos\vartheta = -0.3;\ \phi = 0^o\}$, and another peak of the map occurs around the $\{\cos\vartheta = -0.3;\ \phi = 90^o\}$ point of the map. In these orientations marked here as I_w^C and III_w, respectively, the water molecule is tilted slightly away from the dipole vector from the liquid phase, and stays perpendicular to the liquid surface pointing straight towards the liquid phase by one of its H atoms, respectively. It is also seen that the main orientational preferences do not change in the entire surface layer as well as in its separate zones A, B and C up to moderately low surface water mole fractions. (In the 60% acetone system the mole fraction of the water molecules in the surface layer is too low, being about 0.15 (see Table 3), which makes the corresponding water orientational maps already too noisy.)

In the entire surface layer of neat acetone the molecules again prefer an orientation in which the dipole vector lays close to the parallel alignment with the macroscopic plane of the

surface, *YZ*, as the peak of the $P(\cos\vartheta,\phi)$ orientational map is located around $\{\cos\vartheta = 0.3;\ \phi = 90^o\}$. In this alignment, marked as I_a, the acetone molecule stays perpendicular to the macroscopic plane of the surface, *YZ*, while its dipole vector declines slightly, by about 15-20^o from this plane, pointing flatly towards the vapor phase. This orientation is preferred in the entire surface layer independently from the composition of the system, and also in its zones B and C. In zone A of the surface layer, however, another orientation of the acetone molecules, corresponding to the $\{\cos\vartheta = 0.3;\ \phi = 0^o\}$ point of the orientational map becomes preferred. In this orientation, marked as II_a, the entire molecule is tilted slightly, by about 15-20^o from the parallel alignment with the macroscopic plane of the surface, *YZ*, pointing by the dipole vector flatly towards the vapor phase. The preferred alignments of the molecules I_w, I_w^A, I_w^C, II_w and III_w, and I_a and II_a are illustrated in Figs. 12 and 13, respectively.

To understand the origin of these orientational preferences it should be noted that in neat bulk acetone the neighboring molecules prefer antiparallel dipolar relative alignment, in which the C=O double bonds are close to each other.[3] Furthermore, the apolar CH_3 groups of neighboring molecules also prefer to be located close to each other.[3] As is illustrated in Figure 14, acetone molecules of orientation II_a located at the crests of the wavy surface (zone A) can form similar alignments with their near neighbors of orientation I_a in the troughs (zone C) of the surface. Further, water molecules of alignments I_w^A and II_w in zone A can hydrogen bond to an acetone molecule of alignment I_a in zone C, whereas water molecules of alignments I_w^C and III_w in zone C can form a hydrogen bond with an acetone molecule of orientation I_a in zone A. Finally, a water molecule of alignment I_w^A or II_w in zone A can also form a hydrogen bond with a water molecule of alignment I_w^C or III_w in zone C. All these possible near-neighbor interactions between surface molecules in their preferred alignments are illustrated in Fig. 14. Summarizing, the orientational preferences of the surface molecules are such that two neighboring acetone molecules can adopt relative alignments similar to what is preferred in the bulk liquid phase, and water molecules, being in minority in the surface layer, adopt orientations in which they can form hydrogen bonds with neighboring acetones being in one of their preferred alignments, and also with each other.

Finally, it should be noted that no marked orientational preference of any of the two molecules has been observed neither in the second or third molecular layer beneath the liquid

surface, nor in its separate zones A, B, or C. This finding reflects the fact that the dipole vector of the surface molecules does not prefer strongly tilted alignments relative to the macroscopic plane of the surface, *YZ*, and hence dipole-dipole interaction-driven preferred alignments do not propagate beyond the surface layer. This finding indicates again that, also from this point of view, the second subsurface layer already belongs to the bulk liquid phase of the system.

5. Summary and Conclusions

In this paper we have presented a detailed analysis of the intrinsic liquid surface of acetone-water mixtures of different compositions by means of computer simulation, using a potential model pair that previously proved to be able to excellently reproduce the mixing properties of acetone and water.[17] Our results clearly show that acetone and water molecules have a strong tendency for microscopic separation from each other, forming relatively large self-associates. Thus, acetone molecules are strongly adsorbed at the liquid surface, and this adsorption extends to several molecular layers. Further, like molecules form relatively large lateral self-associates within the surface layer. These findings are in accordance with the fact that the thermodynamic driving force behind the miscibility of acetone and water is very weak,[36] and at large acetone mole fractions it is entirely of entropic origin, i.e., the energy of the mixing is positive.[17,36]

It is also seen that, besides the multi-layer adsorption of the acetone molecules, the effect of the vicinity of the apolar vapor phase extends only to the first molecular layer of the liquid phase. Thus, the surface layer is wider and rougher, and its molecules are less tightly packed, much stronger oriented, and much slower exchanged with the rest of the system than in the subsequent layers. In other words, in all these respects, the second layer beneath the liquid surface is already part of the bulk liquid phase.

Finally, we have found that the orientational preferences of the surface molecules are primarily governed by the dipole-dipole interactions of the neighboring acetone molecules, and by the possibility of the hydrogen bond formation between neighboring acetone-water pairs.

Acknowledgements. This work has been supported by the Hungarian OTKA Foundation under Project No. OTKA 104234.

References

(1) Allen, M. P.; Tildesley, D. J. *Computer Simulation of Liquids*; Clarendon Press: Oxford, 1987.

(2) Evans, G. J.; Evans, M. W. Computer Simulation of Some Spectral Properties of Liquid Acetone. *J. Chem. Soc. Faraday Trans. II* **1983,** *79,* 153-165.

(3) Jedlovszky, P.; Pálinkás, G. Monte Carlo Simulation of Liquid Acetone with a Polarizable Potential model. *Mol. Phys.* **1995,** *84,* 217-233.

(4) Bushuev, Yu. G.; Davletbaeva, S. V.Structural Properties of Liquid Acetone. *Russ. Chem. Bulletin* **1999,** *48,* 25-34.

(5) Martin, M. G.; Biddy, M. J. Monte Carlo Molecular Simulation Predictions for the Heat of Vaporization of Acetone and Butyramide. *Fluid Phase Equilibria* **2005,** *236,* 53-57.

(6) Ghatee, M. H.; Taslimian, S. Investigation of the Temperature and Pressure Dependent Equilibrium and Transport Properties of Liquid Acetone by Molecular Dynamics Simulation. *Fluid Phase Equilibria* **2013,** *358,* 226-232.

(7) Ferrario, M.; Haughney, M.; McDonald, I. R.; Klein, M. L. Molecular-Dynamics Simulation of Aqueous Mixtures: Methanol, Acetone, and Ammonia. *J. Chem. Phys.* **1990,** *93,* 5156-5166.

(8) Bushuev, Yu. G.; Korolev, V. P. Structural Properties of Dilute Aqueous Solutions of Dimethylformamide and Acetone Based on Computer Simulation. *Russ. Chem. Bulletin* **1998,** *47,* 569-577.

(9) Wheeler, D. R.; Rowley, R. R. Shear Viscosity of Polar Liquid Mixtures via Non-Equilibrium Molecular Dynamics: Water, Methanol, and Acetone. *Mol. Phys.* **1998,** *94,* 555-564.

(10) Gomide Freitas, L. C.; Cordeiro, J. M. M.; Garbujo, F. L. L. Theoretical Studies of Liquids by Computer Simulations: The Water-Acetone Mixture. *J. Mol. Liq.* **1999,** *79,* 1-15.

(11) Weerasinghe, S.; Smith, P. E. Kirkwood-Buff Derived Force Field for Mixtures of Acetone and Water. *J. Chem. Phys.* **2003,** *118,* 10663-10670.

(12) Takebayashi, Y.; Yoda, S.; Sugeta, T.; Otake, K.; Sako, T.; Nakahara, M. Acetone Hydration in Supercritical Water: ^{13}C-NMR Spectroscopy and Monte Carlo Simulation. *J. Chem. Phys.* **2004,** *120,* 6100-6110.

(13) Perera, A.; Sokolić, F. Modeling Nonionic Aqueous Solutions: The Acetone-Water Mixture. *J. Chem. Phys.* **2004,** *121*, 11272-11282.

(14) Jedlovszky, P.; Idrissi, A. Hydration Free Energy Difference of Acetone, Acetamide, and Urea. *J. Chem. Phys.* **2008,** *129*, 164501-1-7.

(15) Jedlovszky, P.; Idrissi, A.; Jancsó, G. Can Existing Models Qualitatively Describe the Mixing Behavior of Acetone with Water? *J. Chem. Phys.* **2009,** *130*, 124516-1-8.

(16) Pereyra, R. G.; Asar, M. L.; Carignano, M. A. The Role of Acetone Dipole Moment in Acetone-Water Mixture. *Chem. Phys. Letters* **2011,** *507*, 240-243.

(17) Pinke, A.; Jedlovszky, P. Modeling of Mixing Acetone and water: How Can Their Full Miscibility Be Reproduced in Computer Simulations? *J. Phys. Chem. B* **2012,** *116*, 5977-5984.

(18) Semino, R.; Laria, D. Excess Protons in Water-Acetone Mixtures. *J. Chem. Phys.* **2012,** *136*, 194503-1-10.

(19) Venables, D. S.; Schmuttenmaer, C. A. Structure and Dynamics of Nonaqueous Mixtures of Dipolar Liquids. II. Molecular Dynamics Simulations. *J. Chem. Phys.* **2000,** *113*, 3249-3260.

(20) Kamath G.; Georgiev G.; Potoff J. J. Molecular Modeling of Phase Behavior and Microstructure of Acetone−Chloroform−Methanol Binary Mixtures. *J. Phys. Chem. B* **2005,** *109*, 19463-19473.

(21) Perera, A.; Zoranić, L.; Sokolić, F.; Mazighi, R. A Comparative Molecular Dynamics Study of Water–Methanol and Acetone–Methanol Mixtures. *J. Mol. Liquids* **2011,** *159*, 52-59.

(22) Idrissi, A.; Vyalov, I.; Kiselev, M.; Jedlovszky, P. Assessment of Potential Models of Acetone/CO_2 and Ethanol/CO_2 Mixtures by Computer Simulation and Thermodynamic Integration in Liquid and Supercritical States. *Phys. Chem. Chem. Phys.* **2011,** *13*, 16272-16281.

(23) Gupta, R.; Chandra, A. Single-Particle and Pair Dynamical Properties of Acetone-Methanol Mixtures Containing Charged and Neutral Solutes: A Molecular Dynamics Study. *J. Theor. Comp. Chem.* **2011,** *10*, 261-278.

(24) Idrissi, A.; Polok, K.; Gadomski, W.; Vyalov, I.; Agapov, A.; Kiselev, M.; Barj, M.; Jedlovszky, P. Detailed Insight into the Hydrogen Bonding Interactions in Acetone–Methanol Mixtures. A Molecular Dynamics Simulation and Voronoi Polyhedra Analysis Study. *Phys. Chem. Chem. Phys.* **2012,** *14*, 5979-5987.

(25) Idrissi, A.; Polok, K.; Barj, M.; Marekha, B.; Kiselev, M.; Jedlovszky, P. Free Energy of Mixing Acetone and Methanol: A Computer Simulation Investigation. *J. Phys. Chem. B* **2013,** *117,* 16157-16164.

(26) Picaud, S.; Hoang, P. N. M. Adsorption of Acetone Molecules on Proton Ordered Ice. A Molecular Dynamics Study. *J. Chem. Phys.* **2000,** *112,* 9898-9908.

(27) Hantal, G.; Jedlovszky, P.; Hoang, P. N. M.; Picaud, S. Investigation of the Adsorption Behaviour of Acetone at the Surface of Ice. A Grand Canonical Monte Carlo Simulation Study. *Phys. Chem. Chem. Phys.* **2008,** *10,* 6369-6380.

(28) Semino, R.; Martí, J.; Guárdia, E.; Laria, D. Excess Protons in Mesoscopic Water-Acetone Nanoclusters. *J. Chem. Phys.* **2012,** *137,* 194301-1-8.

(29) Yeh, Y. L.; Zhang, C.; Held, H.; Mebel, A. M.; Wei, X; Lin, S. H.; Shen, Y. R. Structure of the Acetone Liquid/Vapor Interface. *J. Chem. Phys.* **2001,** *114,* 1837-1843.

(30) Pártay, L.; Jedlovszky, P.; Horvai, G. Structure of the Acetone Liquid-Vapor Interface as Seen from Monte Carlo Simulations. *J. Phys. Chem. B* **2005,** *109,* 12014-12019.

(31) Jedlovszky, P.; Jójárt, B.; Horvai, G. Properties of the Intrinsic Surface of Liquid Acetone, as Seen from Computer Simulations. *Mol. Phys.*, in press.

(32) Idrissi, A.; Hantal, G.; Jedlovszky, P. Properties of the Liquid-Vapor Interface of Acetone-Methanol Mixtures, as Seen from Computer Simulation and ITIM Surface Analysis. *Phys. Chem. Chem. Phys.*, in press.

(33) Chen, H.; Gan, W.; Wu, B. H.; Wu, D.; Zhang, Z.; Wang, H. F. Determination of the Two Methyl Group Orientations at Vapor/Acetone Interface with Polarization Null Angle Method in SFG Vibrational Spectroscopy. *Chem. Phys. Letters* **2005,** *408,* 284-289.

(34) Allen, H. C.; Raymond, E. A.; Richmond, G. L. Non-Linear Vibrational Sum Frequency Spectroscopy of Atmospherically Relevant Molecules at Aqueous Solution Surfaces. *Curr. Opin. Coll. Int. Science* **2000,** *5,* 74-80.

(35) Chen, H.; Gan, W.; Wu, B. H.; Wu, D.; Guo, Y.; Wang, H. F. Determination of Structure and Energetics for Gibbs Surface Adsorption Layers of Binary Liquid Mixture. 1. Acetone + Water. *J. Phys. Chem. B* **2005,** *109,* 8053-8063.

(36) Villamañán, M. A.; Van Ness, H. C. Excess Thermodynamic Properties for water/Acetone. *J. Chem. Eng. Data* **1984,** *29,* 429-431.

(37) Jorgensen, W. L.; Briggs, J. M.; Contreras, M. L. Relative Partition Coefficients for Organic Solutes from Fluid Simulations. *J. Phys. Chem.* **1990,** *94,* 1683-1686.

(38) Stubbs, J. M.; Potoff, J. J.; Siepmann, J. I. Transferable Potentials for Phase Equilibria. 6. United-Atom Description for Ethers, Glycols, Ketones, and Aldehydes. *J. Phys. Chem. B* **2004,** *108,* 17596-17605.

(39) Ferrando, N.; Lachet, V.; Boutin, A. Monte Carlo Simulations of Mixtures Involving Ketones and Aldehydes by a Direct Bubble Pressure Calculation. *J. Phys. Chem. B* **2010,** *114,* 8680-8688.

(40) Rick, S. W. A Reoptimization of the Five-Site Water Potential (TIP5P) for Use with Ewald Sums. *J. Chem. Phys.* **2004,** *120,* 6085-6093.

(41) Pártay, L. B.; Hantal, Gy.; Jedlovszky, P.; Vincze, Á.; Horvai, G. A New Method for Determining the Interfacial Molecules and Characterizing the Surface Roughness in Computer Simulations. Application to the Liquid–Vapor Interface of Water. *J. Comp. Chem.* **2008,** *29,* 945-956.

(42) Hantal, Gy.; Darvas, M.; Pártay, L. B.; Horvai, G.; Jedlovszky, P. Molecular Level Properties of the Free Water Surface and Different Organic Liquid/Water Interfaces, as Seen from ITIM Analysis of Computer Simulation Results. *J. Phys.: Condens. Matter* **2010,** *22,* 284112-1-14.

(43) Pártay, L. B.; Jedlovszky, P.; Vincze, Á.; Horvai, G. Properties of Free Surface of Water-Methanol Mixtures. Analysis of the Truly Interfacial Molecular Layer in Computer Simulation. *J. Phys. Chem. B.* **2008,** *112,* 5428-5438.

(44) Pártay, L. B.; Jedlovszky, P.; Horvai, G. Structure of the Liquid-Vapor Interface of Water-Acetonitrile Mixtures As Seen from Molecular Dynamics Simulations and Identification of Truly Interfacial Molecules Analysis. *J. Phys. Chem. C.* **2009,** *113,* 18173-18183.

(45) Pojják, K.; Darvas, M.; Horvai, G.; Jedlovszky, P. Properties of the Liquid-Vapor Interface of Water-Dimethyl Sulfoxide Mixtures. A Molecular Dynamics Simulation and ITIM Analysis Study. *J. Phys. Chem. C.* **2010,** *114,* 12207-12220.

(46) Fábián, B.; Szőri, M.; Jedlovszky, P. Floating Patches of HCN at the Surface of Their Aqueous Solutions – Can They Make "HCN World" Plausible? *J. Phys. Chem. C* **2014,** *118,* 21469-21482.

(47) Pártay, L. B.; Horvai, G.; Jedlovszky, P. Temperature and Pressure Dependence of the Properties of the Liquid-Liquid Interface. A Computer Simulation and Identification of the Truly Interfacial Molecules Investigation of the Water-Benzene System. *J. Phys. Chem. C.* **2010,** *114,* 21681-21693.

(48) Chacón, E.; Tarazona, P. Intrinsic Profiles beyond the Capillary Wave Theory: A Monte Carlo Study. *Phys Rev. Letters* **2003,** *91*, 166103-1-4

(49) Mezei, M. A New Method for Mapping Macromolecular Topography. *J. Mol. Graphics Modell.* **2003,** *21*, 463-472.

(50) Chowdhary, J.; Ladanyi, B. M. Water-Hydrocarbon Interfaces: Effect of Hydrocarbon Branching on Interfacial Structure. *J. Phys. Chem. B.* **2006,** *110*, 15442-15453.

(51) Jorge, M.; Cordeiro, M. N. D. S. Intrinsic Structure and Dynamics of the Water/Nitrobenzene Interface. *J. Phys. Chem. C.* **2007,** *111*, 17612-17626.

(52) Wilard, A. P.; Chandler, D. Instantaneous Liquid Interfaces. *J. Phys. Chem. B.* **2010,** *114*, 1954-1958.

(53) Jorge, M.; Jedlovszky, P.; Cordeiro, M. N. D. S. A Critical Assessment of Methods for the Intrinsic Analysis of Liquid Interfaces. 1. Surface Site Distributions. *J. Phys. Chem. C.* **2010,** *114*, 11169-11179.

(54) Sega, M.; Kantorovich, S.; Jedlovszky, P; Jorge, M. The Generalized Identification of Truly Interfacial Molecules (ITIM) Algorithm for Nonplanar Interfaces. *J. Chem. Phys.* **2013,** *138*, 044110-1-10.

(55) Darvas, M.; Pojják, K.; Horvai, G.; Jedlovszky, P. Molecular Dynamics Simulation and Identification of the Truly Interfacial Molecules (ITIM) Analysis of the Liquid-Vapor Interface of Dimethyl Sulfoxide. *J. Chem. Phys.* **2010,** *132*, 134701-1-10.

(56) Darvas, M.; Pártay, L. B.; Jedlovszky, P.; Horvai, G. Computer Simulation and ITIM Analysis of the Surface of Water-Methanol Mixtures Containing Traces of Water. *J. Mol. Liquids* **2012,** *15*3, 88-93.

(57) Hantal, G.; Cordeiro, M. N. D. S.; Jorge, M. What Does an Ionic Liquid Surface Really Look Like? Unprecedented Details from Molecular Simulations. *Phys. Chem. Chem. Phys.* **2011,** *1*3, 21230-21232.

(58) Lísal, M.; Posel, Z.; Izák, P. Air–Liquid Interfaces of Imidazolium-Based [TF_2N^-] Ionic Liquids: Insight from Molecular Dynamics Simulations. *Phys. Chem. Chem. Phys.* **2012,** *14*, 5164-5177.

(59) Hantal, G.; Voroshylova, I.; Cordeiro, M. N. D. S.; Jorge, M. A Systematic Molecular Simulation Study of Ionic Liquid Surfaces Using Intrinsic Analysis Methods. *Phys. Chem. Chem. Phys.* **2012,** *14*, 5200-5213.

(60) Lísal, M.; Izák, P. Molecular Dynamics Simulations of n-Hexane at 1-Butyl-3-Methylimidazolium bis(Trifluoromethylsulfonyl) Imide Interface. *J. Chem. Phys.* **2013,** *139*, 014704-1-15.

(61) Pártay, L. B.; Horvai, G.; Jedlovszky, P. Molecular Level Structure of the Liquid/Liquid Interface. Molecular Dynamics Simulation and ITIM Analysis of the Water-CCl_4 System. *Phys. Chem. Chem. Phys.* **2008,** *10*, 4754-4764.

(62) Hantal, G.; Terleczky, P.; Horvai, G.; Nyulászi, L.; Jedlovszky, P. Molecular Level Properties of the Water-Dichloromethane Liquid/Liquid Interface, as Seen from Molecular Dynamics Simulation and Identification of Truly Interfacial Molecules Analysis. *J. Phys. Chem. C* **2009,** *113*, 19263-10276.

(63) Sega, M.; Horvai, G.; Jedlovszky, P. Microscopic Origin of the Surface Tension Anomaly of Water. *Langmuir* **2014,** *30*, 2969-2972.

(64) Sega, M.; Horvai, G.; Jedlovszky, P. Two-Dimensional Percolation at the Free Water Surface and its Relation with the Surface Tension Anomaly of Water. *J. Chem. Phys.* **2014,** *141*, 054707-1-11.

(65) Essman, U.; Perera, L.; Berkowitz, M. L.; Darden, T.; Lee, H.; Pedersen, L. G. A Smooth Particle Mesh Ewald Method. *J. Chem. Phys.* **1995,** *103*, 8577-8594.

(66) Hess, B. P-LINCS: A Parallel Linear Constraint Solver for Molecular Simulation. *J. Chem. Theory Comput.* **2008,** *4*, 116-122.

(67) Hess, B.; Kutzner, C.; van der Spoel, D.; Lindahl, E. GROMACS 4: Algorithms for Highly Efficient, Load-Balanced, and Scalable Molecular Simulation. *J. Chem. Theory Comput.* **2008,** *4*, 435-447.

(68) Berendsen, H. J. C.; Postma, J. P. M.; DiNola, A.; Haak, J. R. Molecular Dynamics with Coupling to an External Bath. *J. Chem. Phys.* **1984,** *81*, 3684-3691.

(69) VLE-CALC, http://vle-calc.com

(70) Enders, S; Kahl, H.; Winkelmann, J. Surface Tension of the Ternary System Water + Acetone + Toluene. *J. Chem. Eng. Data* **2007,** *52*, 1072-1079.

(71) Voronoi, G. F. Recherches sur le Paralléloèders Primitives. *J. Reine Angew. Math.* **1908,** *134*, 198-287.

(72) Medvedev, N. N. *The Voronoi-Delaunay Method in the Structural Investigation of Non-Crystalline Systems*, SB RAS: Novosibirsk, 2000, in Russian.

(73) Okabe, A.; Boots, B.; Sugihara, K.; Chiu, S. N. *Spatial Tessellations: Concepts and Applications of Voronoi Diagrams*, John Wiley, Chichester, 2000.

(74) Zaninetti, L. The Voronoi Tessalation Generated from Different Distributions of Seeds. *Phys. Lett. A* **1992,** *165*, 143-147.

(75) Idrissi, A.; Damay, P.; Yukichi, K.; Jedlovszky, P. Self-Association of Urea in Aqueous Solutions: A Voronoi Polyhedron Analysis Study. *J. Chem. Phys.* **2008,** *129*, 164512-1-9.

(76) Chowdhary, J.; Ladanyi, B. M. Surface Fluctuations at the Liquid-Liquid Interface. *Phys. Rev. E* **2008,** *77*, 031609.

(77) Jedlovszky, P.; Vincze, Á.; Horvai, G. New Insight into the Orientational Order of Water Molecules at the Water/1,2-Dichloroethane Interface: A Monte Carlo Simulation Study. *J. Chem. Phys.* **2002,** *117*, 2271-2280.

(78) Jedlovszky, P.; Vincze, Á.; Horvai, G. Full Description of the Orientational Statistics of Molecules Near to Interfaces. Water at the Interface with CCl_4. *Phys. Chem. Chem. Phys.* **2004,** *6*, 1874-1879.

Tables

TABLE 1. Interaction Parameters of the Molecular Models Used.

molecule	interaction site	σ/Å	(ε/k_B)/K	q/e
acetone[a]	H	2.352	11.07	0.09[b]
	C	3.671	40.26	-0.27[b]
	C(=O)	3.564	35.23	0.55[b]
	O	3.029	60.38	-0.55[b]
water[c]	O	3.097	89.64	0
	H	-	-	0.241
	L[d]	-	-	-0.241

[a]Ref. 16.
[b]Values corresponding to neat acetone. The values to be used in acetone-water mixtures can be obtained using eq. 4.
[c]Ref. 40.
[d]Non-atomic interaction site

TABLE 2. Geometry Parameters of the Molecular Models Used.

molecule	bond	bond length (Å)	angle	bond angle (deg)
acetone	C-H	1.111		
	C-C	1.522		
	C=O	1.230		
			H-C-H	108.4
			H-C-C	110.5
			C-C-C	116.0
			C-C=O	122.0
water	O-H	0.957		
	O-L	0.700		
			H-O-H	104.5
			L-O-L	109.5

TABLE 3. Composition of the First Three Molecular Layers and Bulk Liquid Phase of the Systems Simulated (in Acetone Mole Percentage), and Surface Tension of the Systems Simulated

system	bulk liquid phase	first layer	second layer	third layer	γ / mN m^{-1}	
					simulation	experiment[a]
0% acetone	0.0	0.0	0.0	0.0	51.8	71.98
10% acetone	6.2	49.7	13.2	8.0	34.2	39.07
20% acetone	15.8	63.1	26.7	19.1	28.9	32.21
30% acetone	26.1	70.7	37.3	30.9	25.7	29.35
40% acetone	36.2	77.6	50.0	41.6	25.0	27.98
50% acetone	47.0	80.2	57.1	51.7	22.6	27.04
60% acetone	57.3	85.4	68.0	63.2	20.3	26.03
70% acetone	68.8	87.4	71.8	69.4	20.3	25.44
80% acetone	79.2	91.6	81.3	79.3	19.2	24.51
90% acetone	89.8	94.7	89.9	89.2	19.1	23.8
100% acetone	100.0	100.0	100.0	100.0	19.0	23.02

[a]Ref. 70.

TABLE 4. Several Calculated Properties of the First Three Molecular Layers of the Systems Simulated. The Values in Parenthesis Are the Differences of the X_c Values of the Corresponding and Next Subsurface Layers, ΔX_c.

subsurface layer	system	δ/Å	X_c/Å (ΔX_c/Å)	ξ	a/Å	τ/ps	
						acetone	water
first layer	0% acetone	3.7	22.8 (2.8)	1.6	3.8	-	17.5
	10% acetone	4.7	29.2 (3.6)	1.6	4.3	75.1	9.2
	20% acetone	5.8	36.3 (4.0)	1.7	5.4	55.1	9.1
	30% acetone	5.4	43.8 (4.4)	1.7	5.4	46.3	8.6
	40% acetone	5.7	51.4 (4.6)	1.9	6.0	40.4	8.9
	50% acetone	5.9	59.2 (4.9)	2.8	9.0	38.4	10.1
	60% acetone	6.3	67.1 (5.0)	2.4	8.1	35.7	9.5
	70% acetone	6.0	75.1 (4.9)	1.7	5.8	32.3	8.7
	80% acetone	7.5	83.1 (5.2)	1.8	6.1	30.5	9.1
	90% acetone	8.9	91.1 (5.4)	2.5	9.7	31.5	14.7
	100% acetone	6.3	99.1 (5.4)	1.2	3.9	31.3	-
second layer	0% acetone	3.5	20.0 (2.4)	1.5	3.9	-	1.7
	10% acetone	4.6	25.6 (3.2)	0.9	2.7	4.8	2.4
	20% acetone	5.6	32.3 (3.7)	0.9	2.9	4.0	2.0
	30% acetone	5.4	39.4 (4.1)	0.9	3.0	3.5	2.0
	40% acetone	5.6	46.8 (4.4)	1.0	3.1	3.1	1.8
	50% acetone	5.8	54.3 (4.7)	1.0	3.2	3.2	1.8
	60% acetone	6.2	62.1 (4.9)	1.0	3.4	3.0	1.7
	70% acetone	5.8	70.2 (4.9)	1.0	3.4	2.9	1.5
	80% acetone	7.2	77.9 (5.0)	1.0	3.5	2.8	1.6
	90% acetone	8.7	85.7 (5.2)	1.0	3.5	3.0	1.6
	100% acetone	6.0	93.7 (5.3)	1.0	3.6	2.8	-
third layer	0% acetone	3.4	17.6	0.7	2.1	-	1.7
	10% acetone	4.7	22.4	0.9	2.9	4.7	1.8
	20% acetone	5.6	28.6	1.0	3.0	3.89	1.8
	30% acetone	5.6	35.3	1.0	3.1	3.3	1.7
	40% acetone	5.7	42.4	1.0	3.1	3.0	1.6
	50% acetone	5.8	49.6	1.0	3.2	2.9	1.6
	60% acetone	6.1	57.2	1.0	3.3	2.8	1.6
	70% acetone	5.8	65.3	1.0	3.3	3.1	1.6
	80% acetone	7.1	72.9	0.9	3.4	2.6	1.4
	90% acetone	8.6	80.5	0.9	3.4	2.9	1.4
	100% acetone	5.9	88.4	0.9	3.5	2.4	-

Figure legend

Figure 1. Instantaneous equilibrium snapshot of the 10% acetone system, as taken out from the simulation. The molecules belonging to the first, second and third molecular layers beneath the liquid surface are shown by red, green and blue colors, respectively; the molecules located beneath the third molecular layer are shown by grey color. Acetone molecules are always marked by darker, while waters by lighter shades of the respective colors.

Figure 2. Composition of the first (red squares), second (green circles) and third (blue triangles) molecular layers beneath the liquid surface, in terms of acetone mole percentage, as a function of the bulk liquid phase composition. For comparison, the experimental composition of the vapor phase[69] is also shown (empty circles). The lines connecting the points are just guides to the eye. For reference, the bulk liquid phase composition is also indicated (black solid line).

Figure 3. Surface tension of acetone-water mixtures, normalized by that of neat acetone, as a function of the bulk liquid phase composition (in terms of acetone mole percentage), as obtained from our simulations (red asterisks) and from experiment[70] (black line).

Figure 4. VP area distribution of the projections of the centers the surface molecules to the macroscopic surface plane, *YZ*, as obtained in the 0% (black solid lines), 10% (red dashed lines), 20% (green dotted lines), 30% (dark blue dash-dotted lines), 50% (light blue dash-dot-dotted lines), 70% (magenta short dashed lines), and 100% (yellow short dotted lines) acetone systems, when all molecules are taken into account (top panel), only acetone molecules are taken into account while waters are disregarded (middle panel), and only water molecules are taken into account while acetones are disregarded (bottom panel). To emphasize the exponential decay of the large *A*-side tail of some of the curves, the distributions are shown on a logarithmic scale. The inset shows the VP area distributions in the 10% acetone system, obtained by taking into account both the water and the acetone molecules (solid line), only the acetone molecules (full circles), and only the water molecules (open circles) in the analysis. To emphasize the Gaussian character of some of the curves, these distributions are shown on a linear scale.

Figure 5. Instantaneous equilibrium snapshot of the projections of the centers of the acetone (green) and water (red) molecules into the macroscopic surface plane, *YZ*, as taken out from the simulations of the 10% (left) and 50% (right) acetone systems.

Figure 6. Number density profile of the water (top panel) and acetone (second panel) molecules, and mass density profile of the entire system (third panel) and its first molecular layer beneath the liquid surface (bottom panel) along the macroscopic surface normal axis, *X*, as obtained in the 0% (black full circles), 10% (red solid lines), 40% (blue dashed lines), 70% (green dash-dotted lines), and 100% (open circles) acetone systems. All the profiles shown are averaged over the two liquid-vapor interfaces present in the basic simulation box.

Figure 7. Mass density profile of the entire system (black solid lines) as well as its first (red full circles, second (blue open circles), and third (green asterisks) molecular layers beneath the liquid surface along the macroscopic surface normal axis, *X*, as obtained in the 10% (top panel), 40% (second panel), 60% (third panel), and 90% (bottom panel) acetone systems. All the profiles shown are averaged over the two liquid-vapor interfaces present in the basic simulation box.

Figure 8. Number density profile of the acetone (red solid lines) and water (blue dashed lines) molecules belonging to the surface layer of the 10% (top left panel), 40% (top right panel), 60% (bottom left panel), and 90% (bottom right panel) acetone systems. The scales on the left and right correspond to the acetone and water number densities, respectively. All the profiles shown are averaged over the two liquid-vapor interfaces present in the basic simulation box.

Figure 9. Average normal distance of two surface points, $\overline{d}$, as a function of their lateral distance, *l*, as obtained in the 10% (black squares), 20% (red circles), 40% (green up triangles), 60% (blue down triangles), and 80% (orange stars) acetone systems. The inset shows the $\overline{d}(l)$ data obtained in the first (asterisks), second (open circles), and third (full circles) molecular layers beneath the liquid surface of the 70% acetone system.

Figure 10. Survival probability of the acetone (top panel) and water (bottom panel) molecules in the surface layer of the 0% (black squares), 10% (red circles), 20% (green up triangles), 40% (dark blue down triangles), 70% (light blue diamonds), and 100% (magenta stars) acetone systems. The inset shows the survival probability of the acetone and water molecules in the first (black circles), second (red circles) and third (green circles) molecular layers of the 50% acetone system. To emphasize the exponential decay of the survival probability data, the inset shows them on a logarithmic scale. Full and open symbols always correspond to the acetone and water molecules, respectively.

Figure 11. Definition of the local Cartesian frames fixed to the individual (a) acetone and (b) water molecules, and of the polar angles ϑ and ϕ describing the orientation of the surface normal vector, $\underline{X}$, pointing, by our convention, from the liquid to the vapor phase, in these frames. (c) Illustration of the division of the surface layer into separate zones A, B and C according to the mass density profile of the surface molecular layer.

Figure 12. Orientational maps of the surface water molecules in the systems containing 0% (top row), 10% (second row), 40% (third row), and 60% (bottom row) acetone. The first column corresponds to the entire surface layer; the second, third and fourth column correspond to its separate zones C, B, and A, respectively. Lighter shades of grey denote higher probabilities. The preferred orientations of the water molecules are also illustrated at the bottom of the Figure (O and H atoms are shown by red and light grey colors, respectively, $\underline{X}$ is the surface normal vector pointing towards the vapor phase.)

Figure 13. Orientational maps of the surface acetone molecules in the systems containing 10% (top row), 40% (second row), 60% (third row), and 100% (bottom row) acetone. The first column corresponds to the entire surface layer; the second, third and fourth column correspond to its separate zones C, B, and A, respectively. Lighter shades of grey denote higher probabilities. The preferred orientations of the acetone molecules are also illustrated at the bottom of the Figure (O and C atoms are shown by red and grey colors, respectively, H atoms are omitted for clarity, $\underline{X}$ is the surface normal vector pointing towards the vapor phase.)

Figure 14. Illustration of the interfacial and near neighbor relative orientational preferences of the surface acetone and water molecules, located at surface portions of different local curvatures. C, H, and O atoms are indicated by grey, light grey and red colors, respectively, acetone H atoms are omitted for clarity. The acetone dipole vectors, domains of nearby CH_3 groups and hydrogen bonds are indicated by thick arrows, circles and dashed lines, respectively. $\underline{X}$ is the surface normal vector pointing towards the vapor phase.

Figure 1.

Fábián et al.

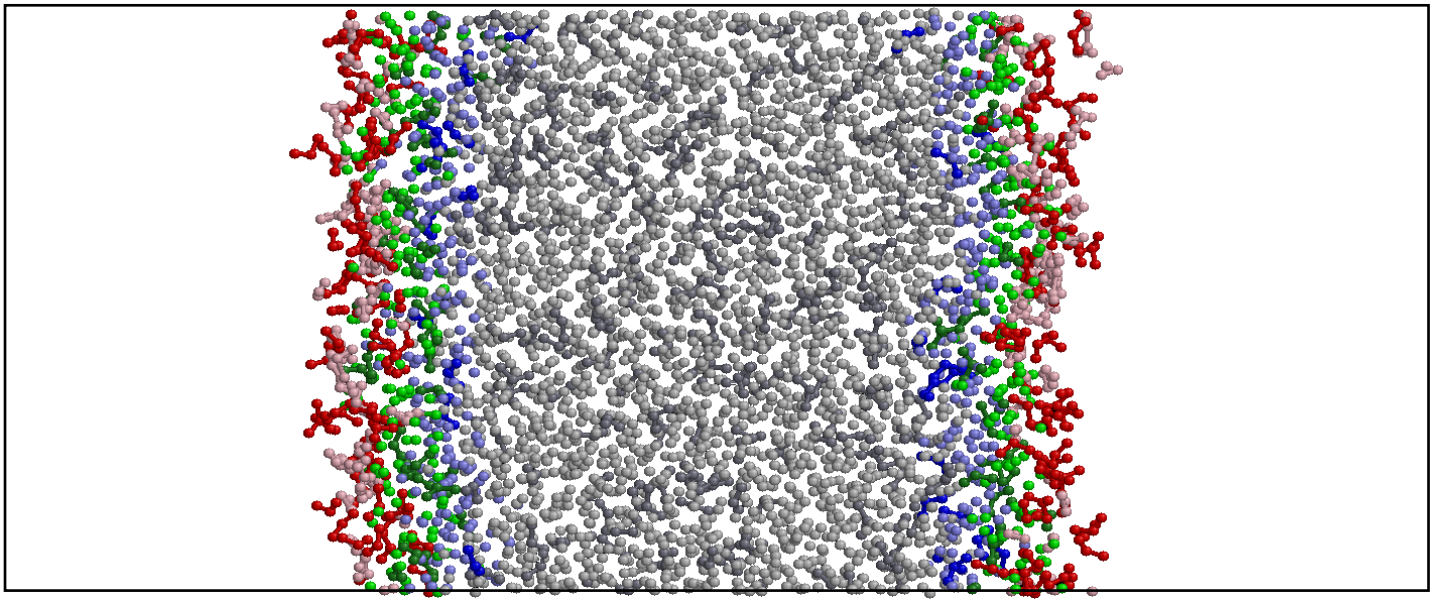

Figure 2.

Fábián et al.

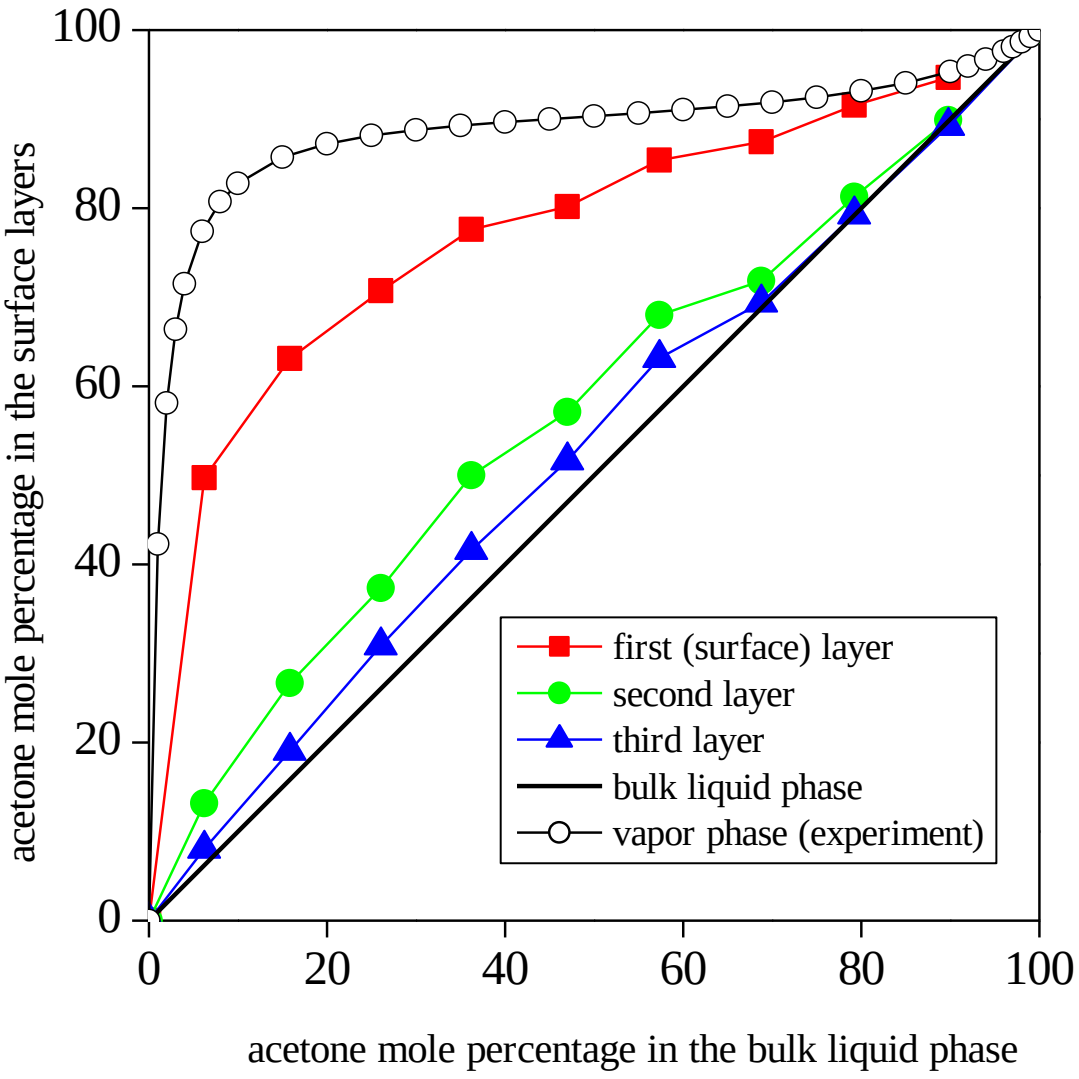

Figure 3.

Fábián et al.

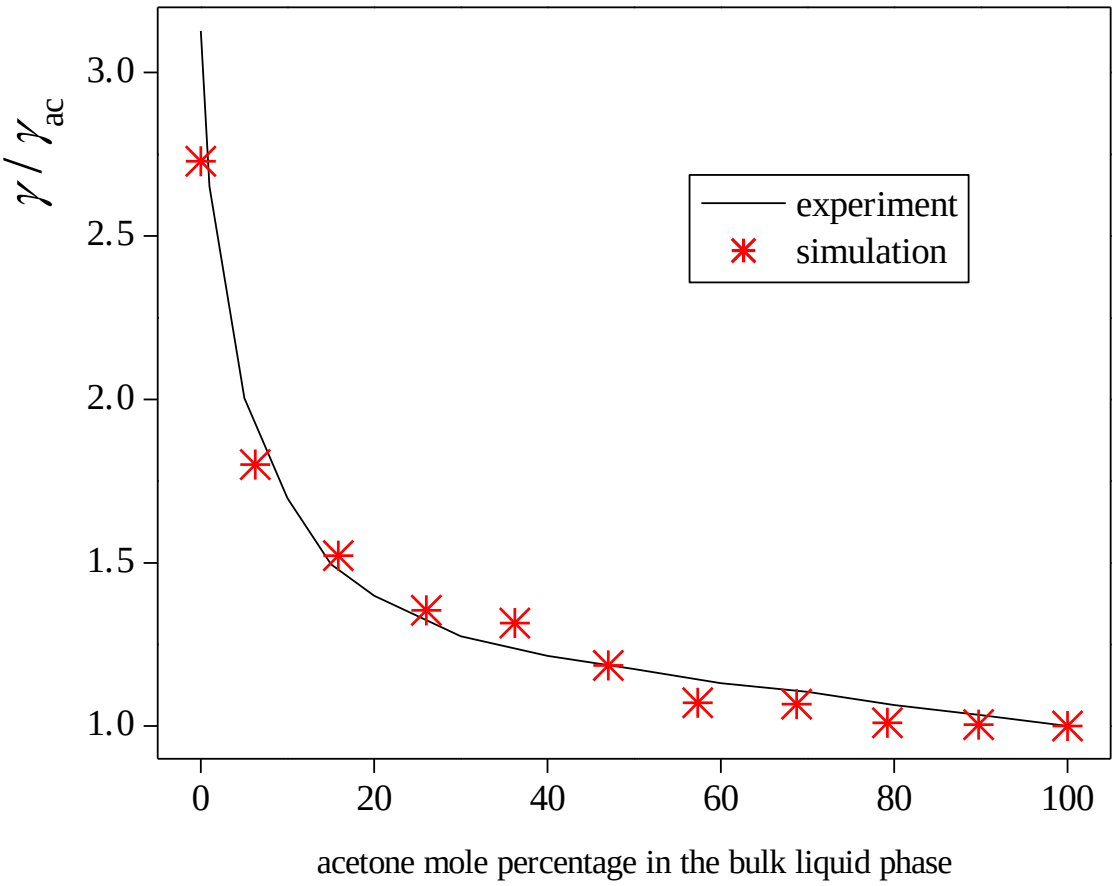

Figure 4.

Fábián et al.

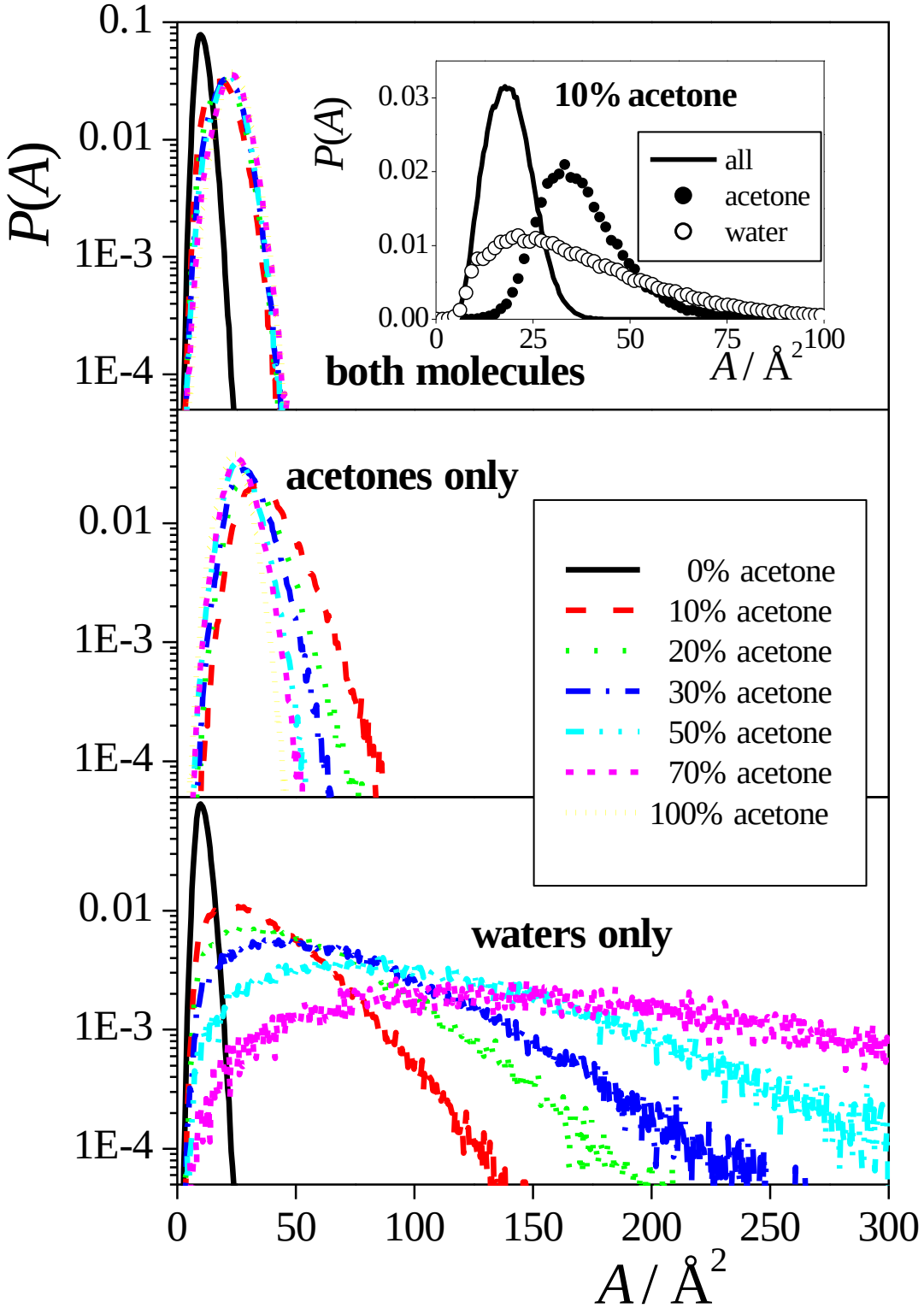

Figure 5.

Fábián et al.

10% acetone system

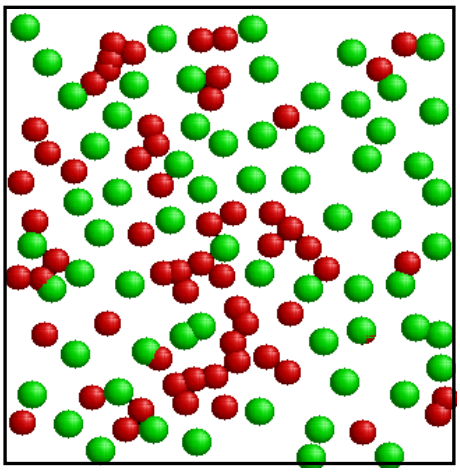

50% acetone system

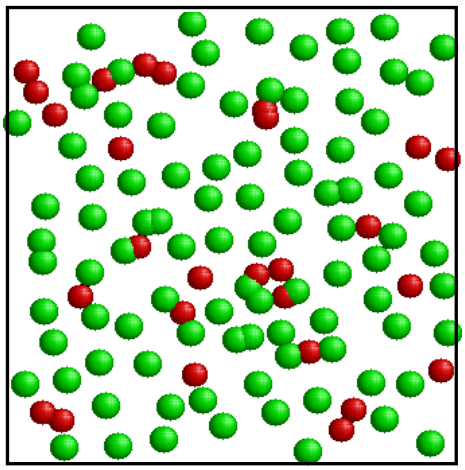

Figure 6.

Fábián et al.

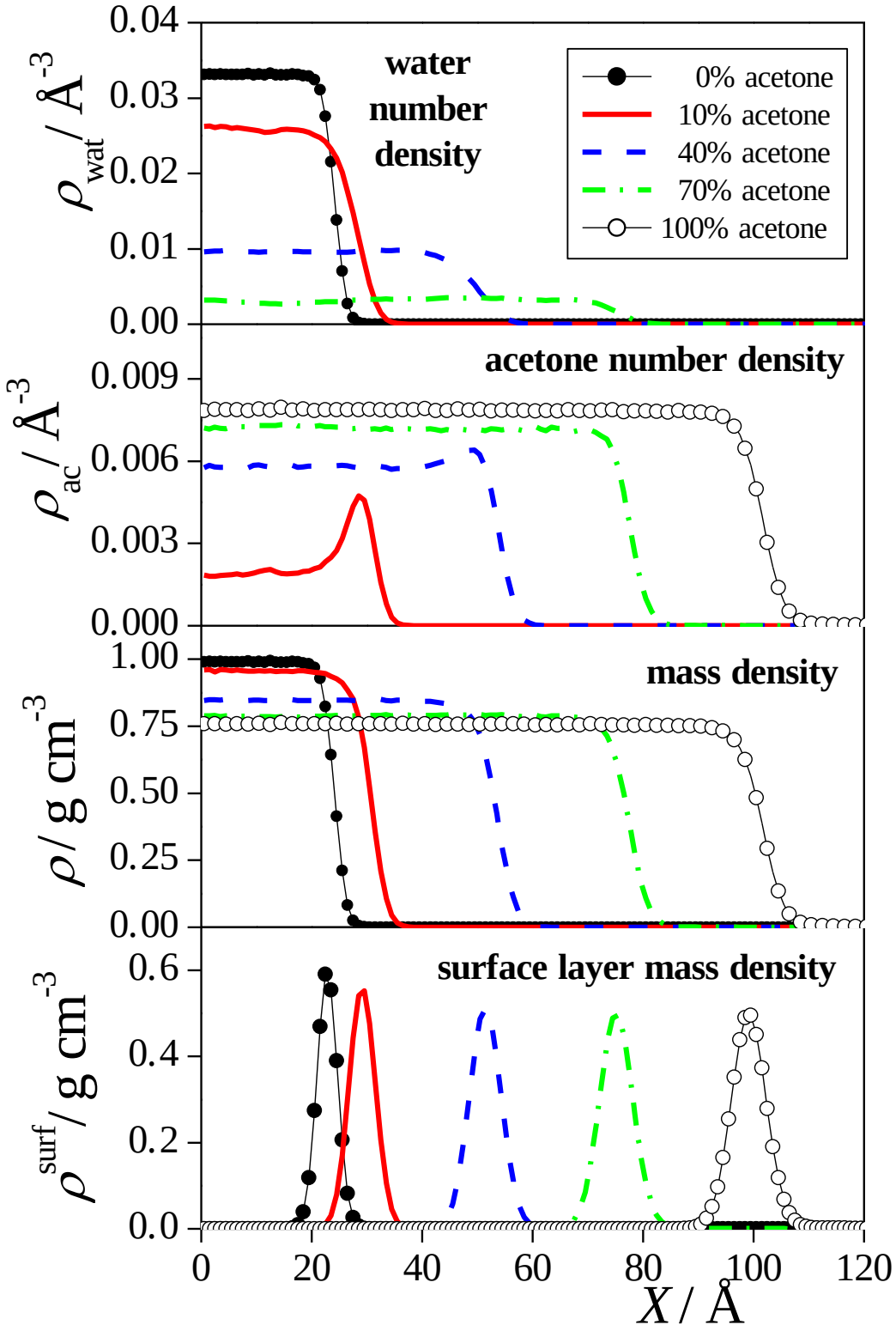

Figure 7.

Fábián et al.

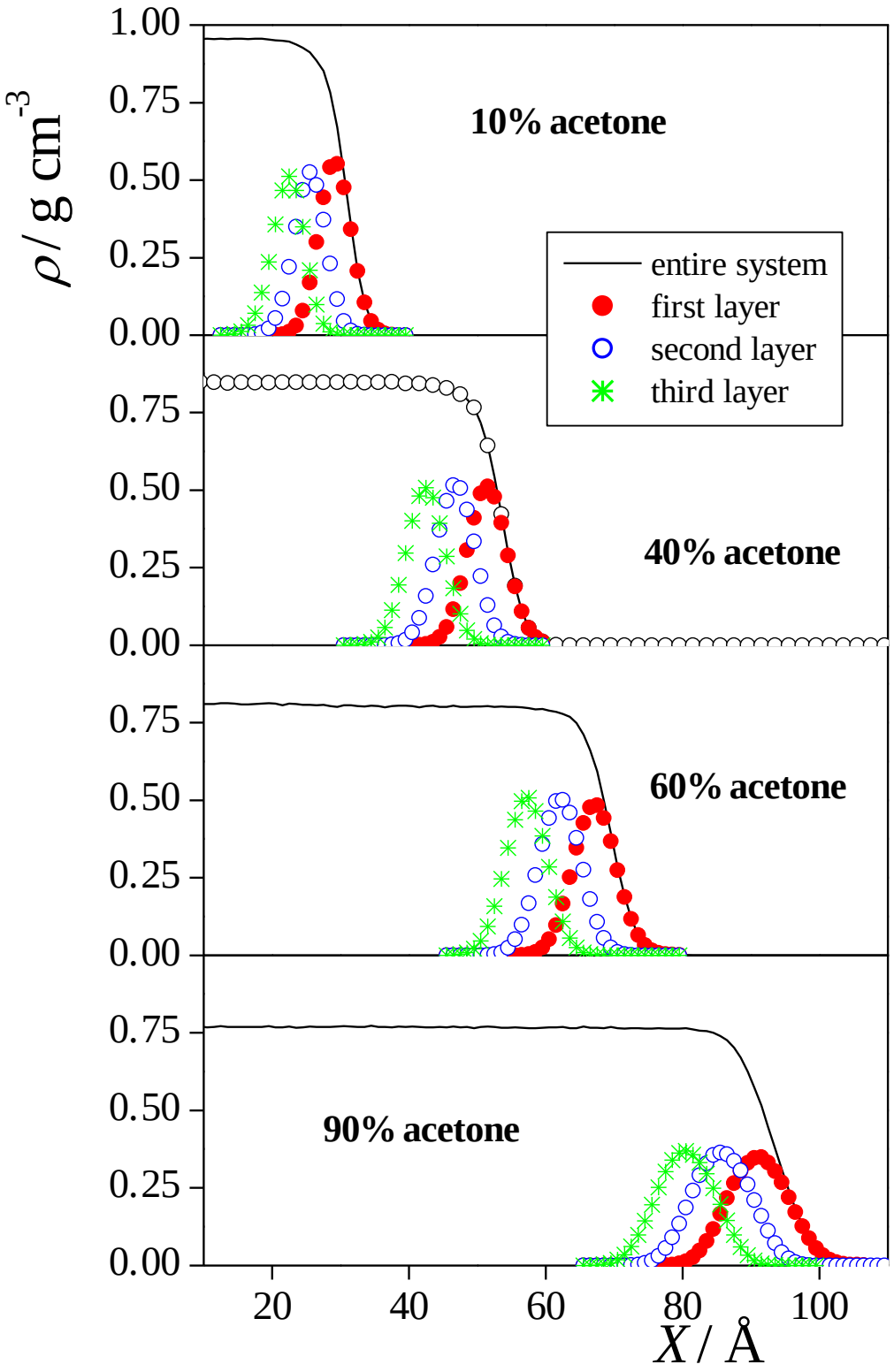

Figure 8.

Fábián et al.

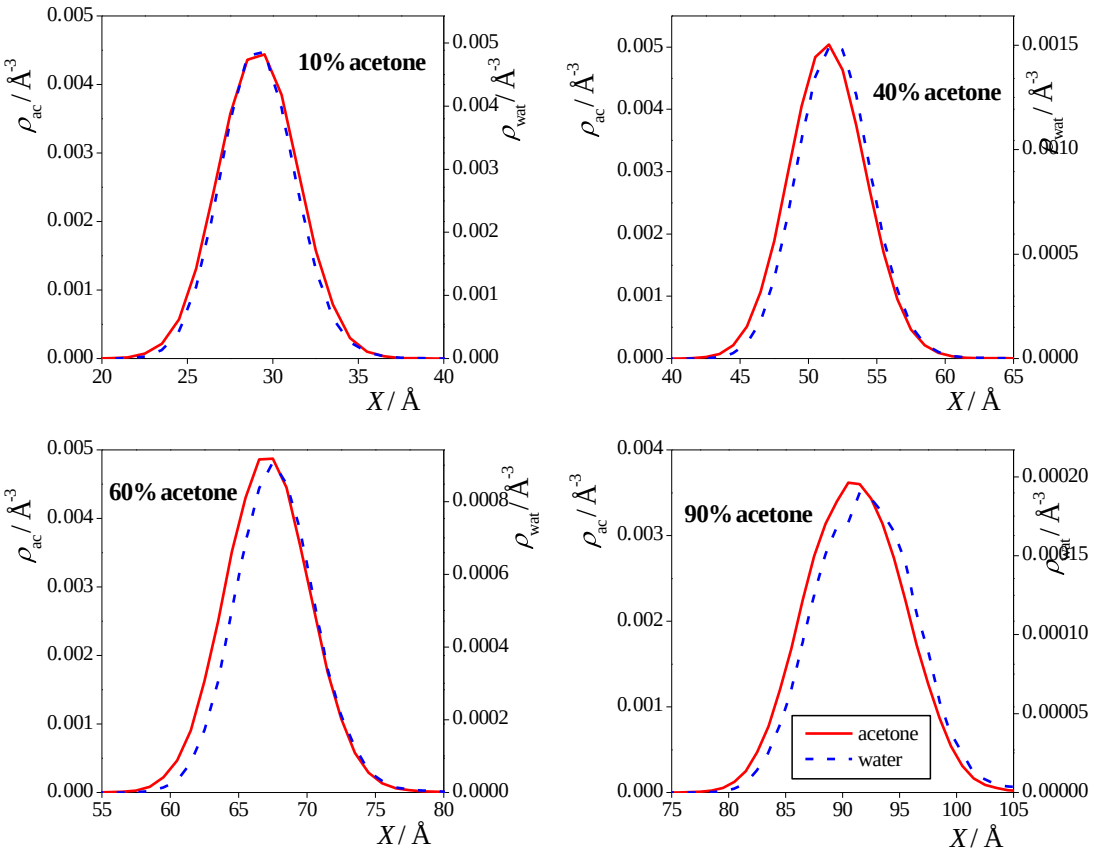

Figure 9.

Fábián et al.

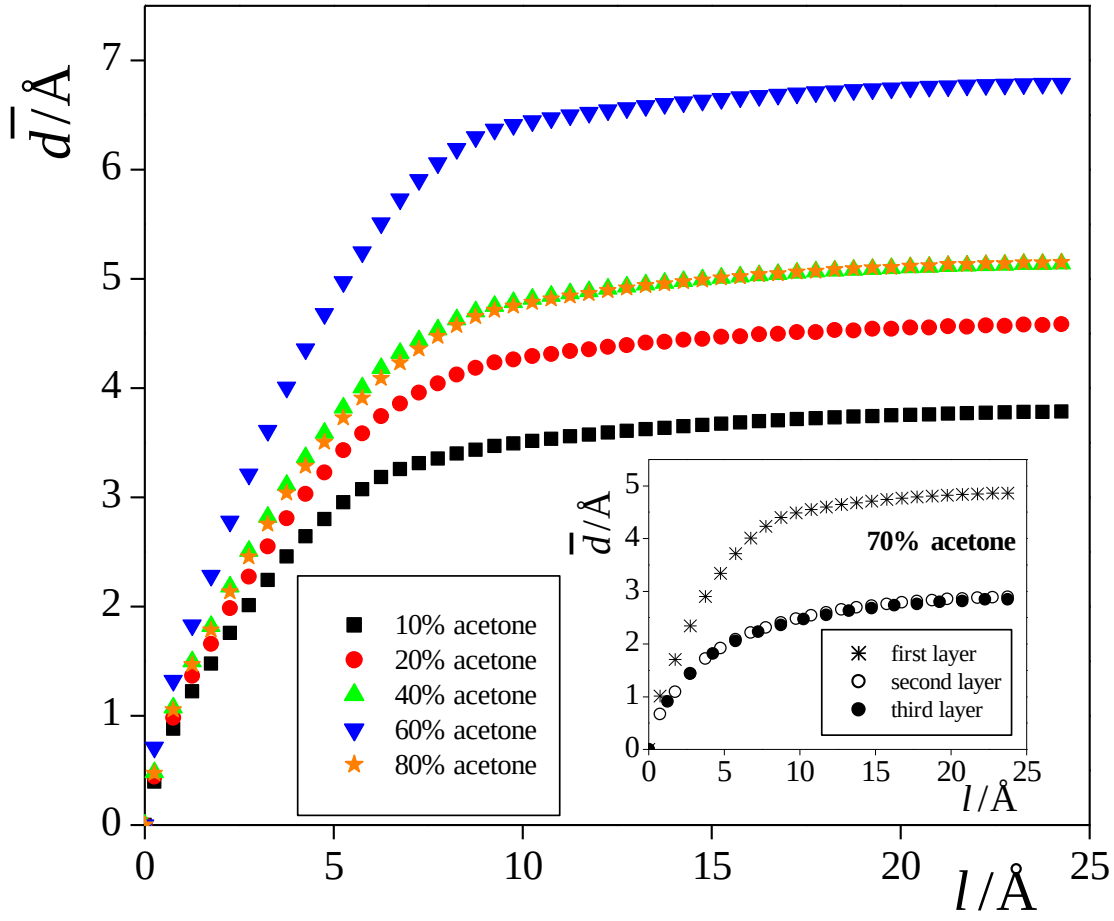

Figure 10.

Fábián et al.

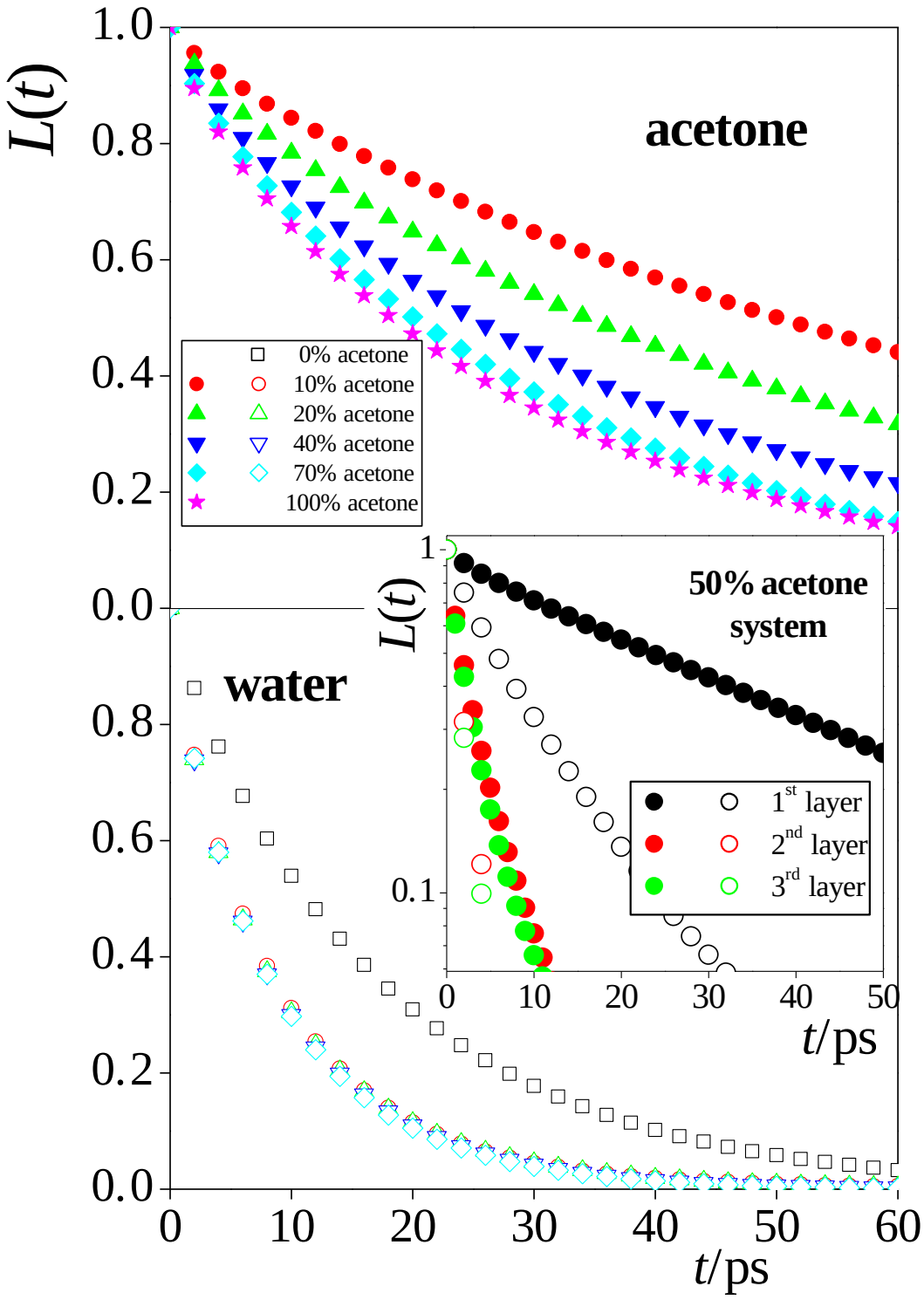

Figure 11.

Fábián et al.

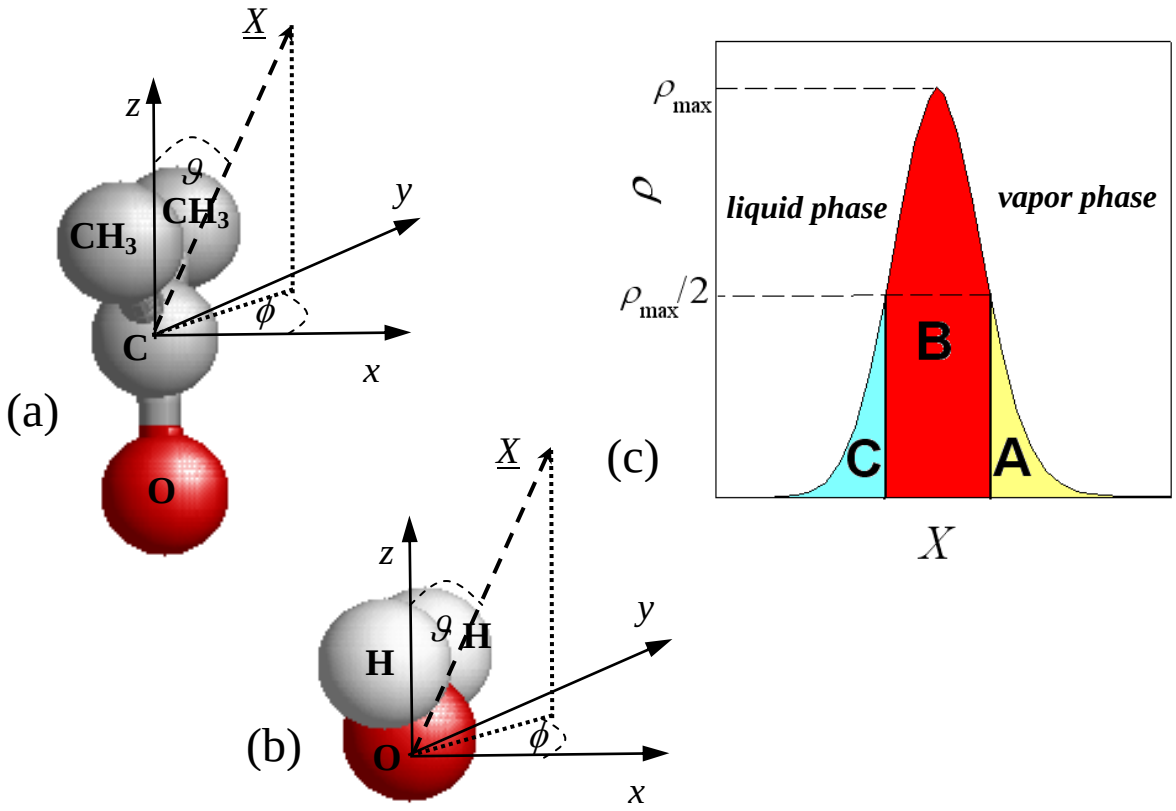

Figure 12.

Fábián et al.

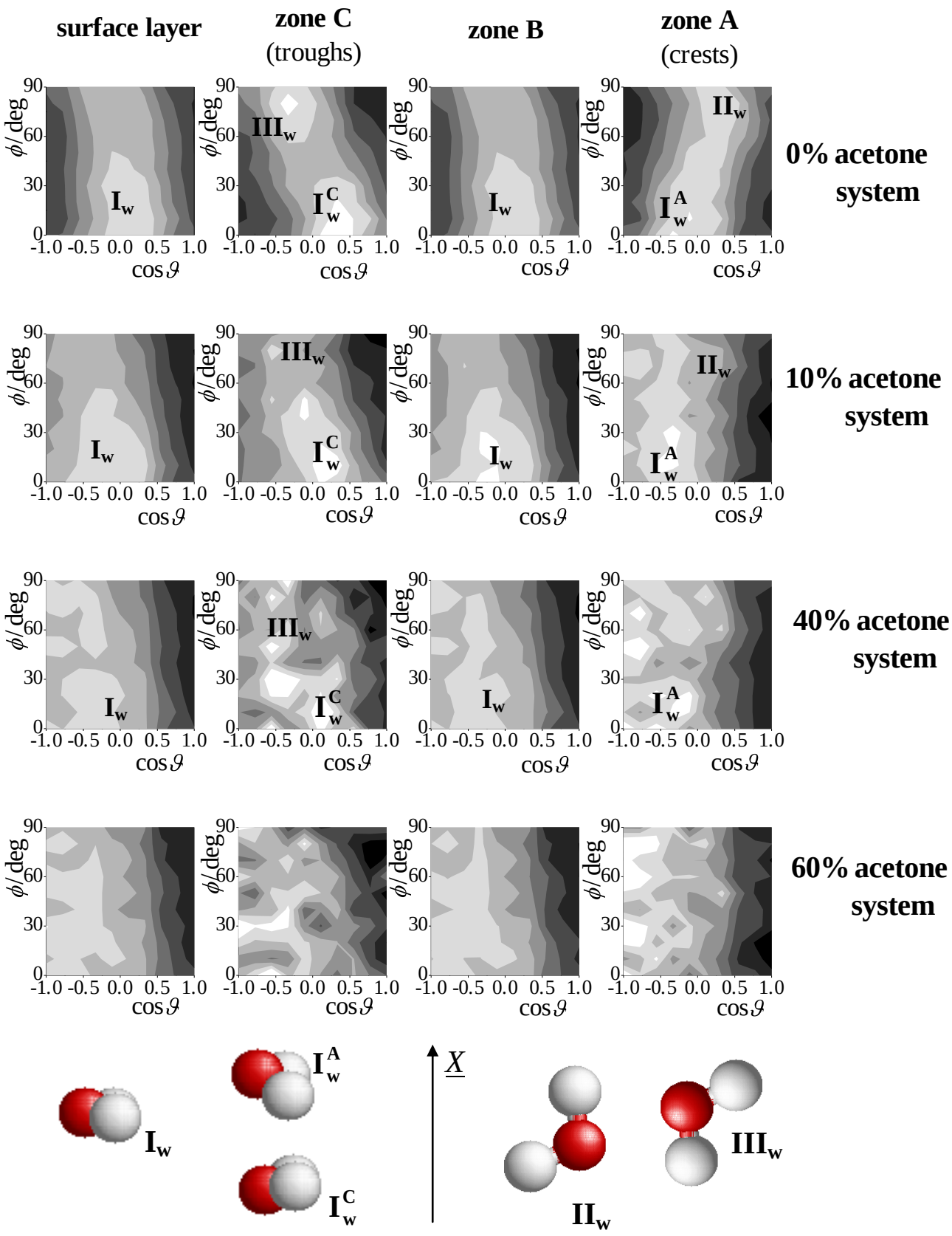

Figure 13.

Fábián et al.

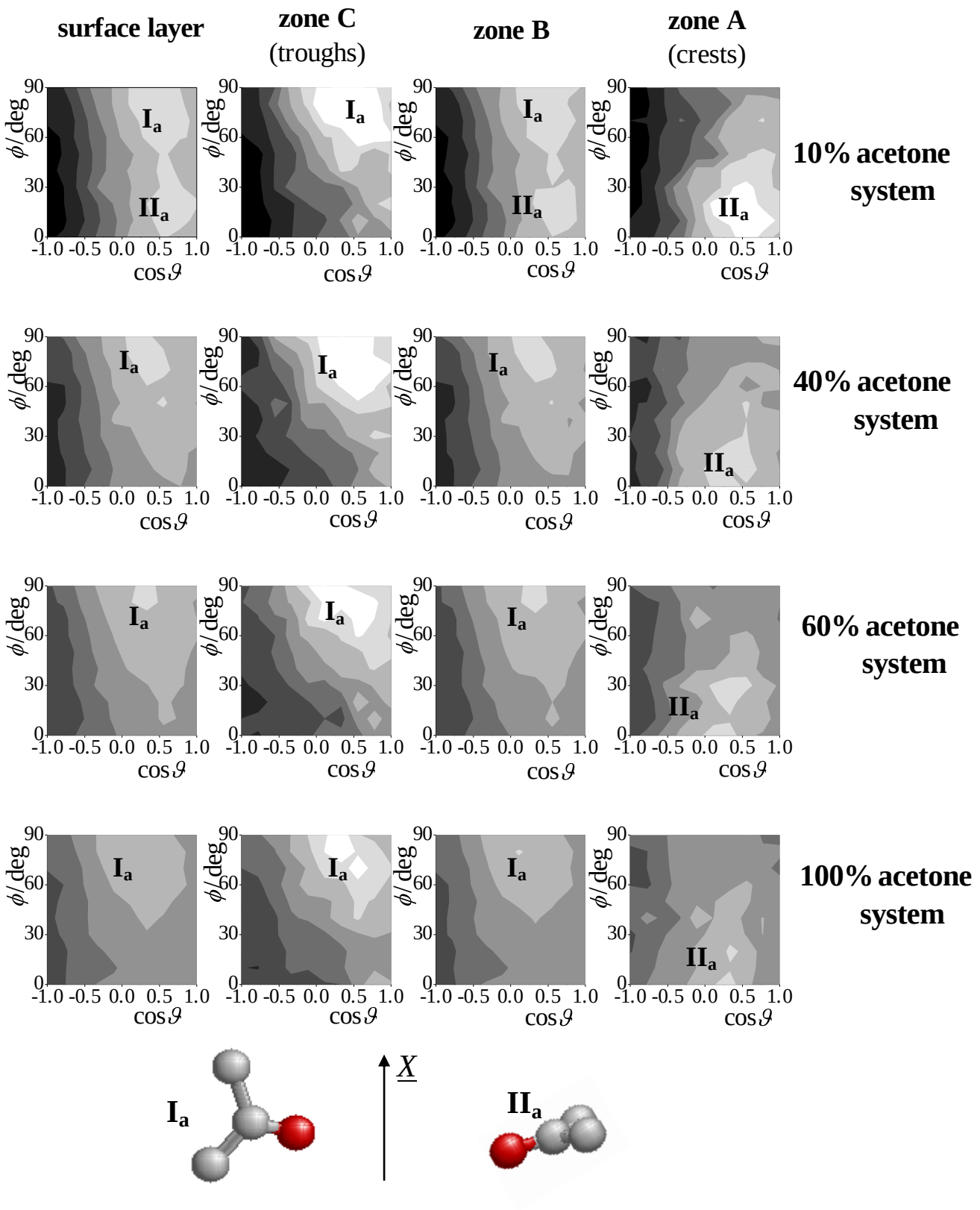

Figure 14.

Fábián et al.

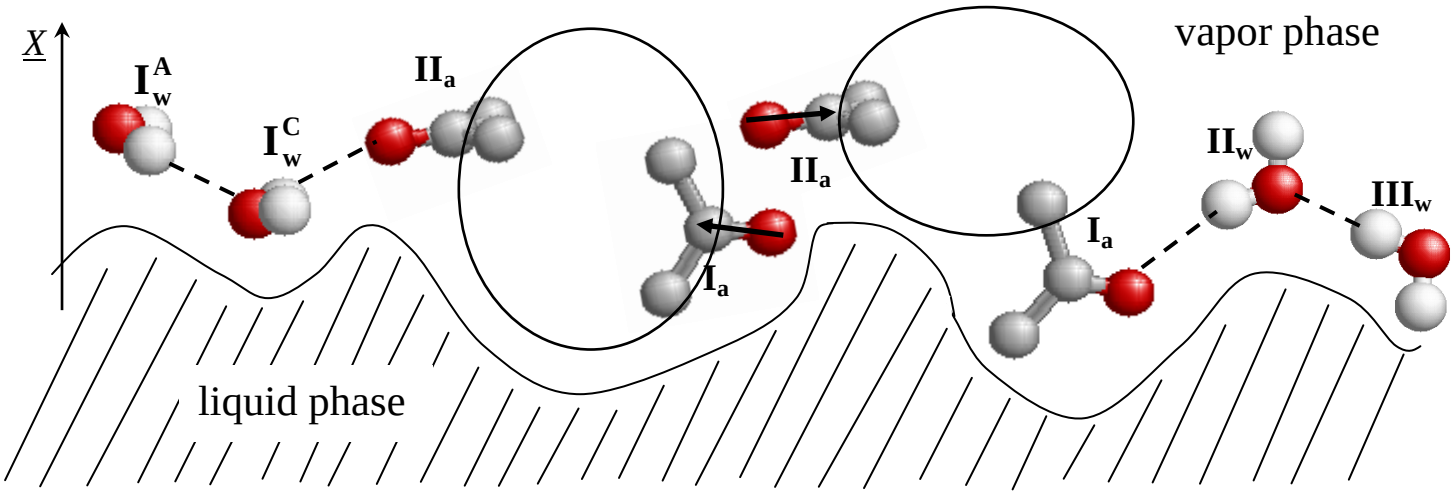

Table of Contents Graphics: